Dear Markus Hrachowitz,

Please find our newest submission of the manuscript, "*Relating seasonal dynamics of enhanced vegetation index to the recycling of water in two endorheic river basins in northwest China*". We have tried to address many of the reviewers' remaining comments. Our point-by-point responses to the reviewers' comments are included below. We hope you find our newest revision suitable for publication.

Best regards,

Charles P.-A. Bourque

Editor

Both reviewers agree that the manuscript has been substantially improved and the results from the analysis now much better supports the interpretation/conclusions. Before publication I would nevertheless strongly encourage the authors to address the remaining reviewer comments. In particular, I would appreciate a short discussion on effect of temperature on the vegetation and its influence on the time lag as suggested by reviewer #2.

Our Response: Sorry for overlooking the reviewer's comment; we had many significant changes to make during our last revision and inadvertently forgot to address the comment. Temperature and soil moisture are both important to plant growth. Deficiencies in either variable can cause disruptions/delays in plant growth. In arid environments (where evaporation >> precipitation), soil moisture is generally the more limiting variable, and as a result our initial submissions tended to focus more on water then on the other variables. For the growing season to start both temperature & soil water need to be favourable. In humid areas, the growing season is mostly controlled by temperature, as soil water is generally not a problem. In arid environments, both variables are equally important, with soil moisture being at times more problematic. We have added text to address the importance of temperature (w.r.t. growing degree-days) & soil water concerning the start of the growing season.

In addition, reviewer #1 raises the concern that the conclusions made still remain too strong and that they should either be further substantiated by additional data (e.g. wind directions) or toned down to some extent, also discussing potential alternative explanations and highlighting pitfalls in the given explanation.

Our Response: We have toned down our claim. We are unaware of alternative explanations that would be consistent with all of the results that we and others have accumulated on this topic in the past several years. We plan to carry this work farther by conducting an isotopic study of the phenomenon.

Finally, CCM seems to be a robust tool to detect causality. It however remains a rather new concept, which may be unknown to many in the community. I would therefore suggest to add some more details about the method, including what exactly was done and what the results (e.g. the figures) show - as i see it, now an interpretation of the figures is given, but it is not fully clear how this interpretation was obtained (i.e. *what can actually be seen in the figures).
Our Response: We incorporate some description in the caption of Fig. 5, along with description in the main body of the manuscript. The method is available in open-sourced R-language modules that can be accessed by those interested in conducting such analysis. For the theory behind the method, I would suggest the readers refer to the papers we cite in the manuscript.

Reviewer No. 1

I appreciate the substantial revisions that the authors have made. I agree that the authors raise an interesting hypothesis and possible explanation for the seasonal dynamics. But I am still somewhat disappointed that the authors did not reply to my alternative explanation for the causal relation for the observed time lag:"this time lag is quite normal in many places in the world. Vegetation development often predates the onset of rain. Moreover temperature depends on elevation. Vegetation will only start to develop when the temperature is above a minimum value. The temperature in the lowland is several degrees higher than in the mountains where vegetation starts later in the season." I had expected a reply to that. The rebuttal that they use GCM's to demonstrate the cause-effect relation is not very convincing, I think.

But having said that, the paper contains sufficient interesting material for publication.
Our Response: See our response to the Editor.

Reviewer No. 2

General comments
The revision is a significant improvement over the first manuscript version: the introduction is now relevant and well referenced, the paper is better structured and easier to follow, and the convergent cross mapping is introduced to solve the causality issue. However, I am still concerned about the claim on 90 % recycling ratio and hope the authors can address it.

The authors claim in the abstract that “Comparison of water volumes associated with in-mountain production of rainfall and snowmelt with that associated with evaporation in the oases revealed that about ~90% of the water flowing downslope to the oases was eventually returned to the Qilian Mountains as water vapour generated in the lowlands”. It seems, thus, that the authors base this claim entirely on the fact that the amount of the basin-wide precipitation and snowmelt correspond to about 90 % of the basin-wide evaporation. Possibly, the authors mean that wind directions, lack of nearby oases, bidirectional feedback based on convergent cross mapping, and

orographic lifting may be indicative of a high recycling ratio. Comparison of water volumes is not sufficient to reveal the level of recycling. Because, theoretically, the amount of precipitation and snowmelt in the mountains could very well match the amount of oases evaporation, even if **all** evaporation from the oases would leave the river basin and **all** precipitation in the mountains would be fed by evaporation from elsewhere. It seems to me that it may be valid to claim that oases evaporation is likely to be important for mountain precipitation, but not valid to claim that the returning flow amounts to about 90 %. If the wind directions, orographic precipitation, and surrounding deserts **exclude** the possibility of significant external contribution, the authors should emphasize and elaborate on that to avoid misunderstandings. Perhaps the authors could consider to either clarify and strengthen their arguments, or soften their claim? (In fact, in the conclusion, the authors use the wording "seems to indicate" instead of "reveal", which is at the other end of the uncertainty/certainty terminology scale.)

Our Response: Given the lack of daily wind data to confirm our point, we've decided to tone down the claim. We will continue examining this phenomenon at a later time, but from an isotopic perspective.

Specific or technical comments

L.156-162: The units for different water flows are sometimes kg m-2 y-1 and sometimes m3 y-1.

Our Response: "kg m^{-2} $month^{-1}$" is used when referring to fluxes, and "m^3 $month^{-1}$" when referring to monthly volumes.

L.371-372: Why "0.0" and not just "0"?

Our Response: Changed as requested.

L. 401-402: For clarity, perhaps specify which "related timeseries" and/or "paired variables" you refer to.

Our Response: We now specify the variables.

Fig. 8: The legend for (c) and (d) did not include the circled and boxes for direct rainfall and snowmelt.

Our Response: We've corrected the problem.

The reference Clark et al. 2014 should be 2015.

Our Response: Thank you picking up this error.

Regarding colour blind friendly colour schemes, see for example: Light and Bartlein (2004) The End of the Rainbow? Color Schemes for Improved Data Graphics. Eos, Vol. 85, No. 40. Available from: http://geography.uoregon.edu/datagraphics/EOS/Light-and-Bartlein_EOS2004.pdf

Our Response: We have tried to improve the colouring and labelling in the figures so that colour-blind readers can benefit from the publication. Many of the colour schemes we use are based on the Light and Bartlein paper. We thank the reviewer for the reference.

Relating seasonal dynamics of enhanced vegetation index to the recycling of water in two endorheic river basins in northwest China

Mir A. Matin[1] and Charles P.-A. Bourque[1,2]

[1] {Faculty of Forestry and Environmental Management, University of New Brunswick, New Brunswick, Canada}

[2] {School of Soil and Water Conservation, Beijing Forestry University, Beijing, PR China}

Correspondence to: Charles P.-A. Bourque (cbourque@unb.ca)

Abstract

This study associates the dynamics of enhanced vegetation index in lowland desert oases to the recycling of water in two endorheic (hydrologically-closed) river basins in Gansu Province, (northwest China), along a gradient of elevation zones and landcover types. Each river basin was subdivided into four elevation zones representative of (i) oasis plains and foothills, and (ii) low-, (iii) mid-, and (iv) high-mountain elevations. Comparison of monthly vegetation phenology with precipitation and snowmelt dynamics within the same basins over a 10-year period (2000-2009) suggested that the onset of the precipitation season (cumulative % precipitation > 7-8%) in the mountains, typically in late April to early May, was triggered by the greening of vegetation and increased production of water vapour at the base of the mountains. Seasonal evolution of in-mountain precipitation correlated fairly well with the temporal variation in oasis-vegetation coverage and phenology characterised by monthly enhanced vegetation index, yielding coefficients of determination of 0.65 and 0.85 for the two basins. Convergent cross mapping of related timeseries indicated bi-directional causality (feedback) between the two variables.

Comparisons between same-zone monthly precipitation amounts and enhanced vegetation index provided weaker correlations. Start of the growing season in the oases was shown to coincide with favourable spring warming and ~~with the~~ discharge of meltwater from ~~the~~ low- to mid-elevations of the Qilian Mountains (Zones 1 and 2) in mid-to-late March. ~~Mid~~In terms of plant need for water, mid-seasonal development of oasis vegetation was seen to be controlled to a greater extent by the production of rain in the mountains. Comparison of water volumes associated with in-~~mountain~~ basin production of rainfall and snowmelt with that associated with evaporation ~~in the oases revealed~~ seemed to suggest that about 90% of the available liquid water (i.e., mostly in the form of direct rainfall and snowmelt in the mountains) ~~flowing downslope to the oases was eventually returned to the Qilian Mountains as water vapour generated in the lowlands~~was recycled locally.

1 Introduction

River basins not connected to oceans (endorheic basins; Meybeck, 2003) occupy about 13% of the total land surface of the earth (Meybeck et al., 2001) and generate about 2.3% of global runoff (Shiklomanov, 1998). Most of these basins are located in water-limited regions of the world, generally in the middle of continents remote from oceanic sources of atmospheric moisture or blocked by mountain ranges (Meybeck et al., 2001; Warner, 2004). Rivers associated with endorheic basins in northwest China are typically sourced by precipitation forming in mountains. These rivers commonly terminate in deserts as a result of strong evaporation (Li et al., 2013b). Endorheic basins are extremely sensitive to landcover and climate variability (Meybeck, 2003). Therefore, understanding the water cycle in these areas is extremely important for the long term sustainability (Pilgrim et al., 1988) of desert oases in northwest China.

Formatted: Left

The study of water recycling in the hyper-arid lowlands of northwest China has been largely centred on hydro-geochemical and isotopic analyses of precipitation and surface and subsurface water (e.g., Gates et al., 2008a; Ma et al., 2008; Ma et al., 2009; Ma et al., 2012; Huang and Wen, 2014) and atmospheric-circulation modelling studies (e.g., Gao et al., 2004; Chu et al., 2005; Meng et al., 2009; Meng et al., 2012; Wen et al., 2012; Meng et al., 2015). ~~In general,~~ Many of these studies ~~concern~~ involve coarse spatiotemporal resolutions.

Based on geologic, isotopic, and atmospheric circulation studies, aridification of northwest China has been theorised to have started about 12 Ma (mega-annum or million years) ago following (i) withdrawal of the Paratethys Sea from central Asia, resulting in loss of a major source of moisture; (ii) building of the Himalayas and southcentral Qinghai-Tibet Plateau, obstructing moisture-carrying airmasses from oceanic source-areas in the south (i.e., southeast Asian monsoon); and (iii) outward expansion of the northern fringe of the Qinghai-Tibet Plateau and subsequent growth of the Tian and Pamir Mountain ranges to the northwest of the Plateau (Kent-Corson, 2009; Zhuang et al., 2011), giving rise to the vast Taklamakan Desert (Tarim Basin, Xinjiang Province; inset in Fig. 1). Regional climate along the northern fringe of the Qinghai-Tibet Plateau, particularly along the Hexi Corridor of westcentral Gansu Province (inset, Fig. 1), is mostly controlled by the dry Central Asian airmass (Kent-Corson, 2009). Westerly airflow associated with this airmass interacts with numerous mountain ranges between the Caspian Sea to the Tian Mountains in the west of the Hexi Corridor (Warner, 2004). These interactions cause the moisture in the air to progressively lessen as the airmass continues to track eastward towards the Hexi Corridor and Qilian Mountains (Fig. 1). External contribution of moisture to the Hexi Corridor from Europe and western Asia (Warner, 2004; van der Ent et al.,

2010) is anticipated to be low and of marginal importance to the localised recycling of water in westcentral Gansu.

<Fig.1>

Formatted: Font: Bold

Formatted: Centered

The Hexi Corridor is renowned for its excessive dryness and large oases along the base of the Qilian Mountains, most notably the Liangzhou, Minqin, and Zhangye Oases (Fig. 1). Oases in the area provide important refugia to flora, fauna, and humans alike. Oases in northwest China occupy about 5% of the total land mass of the region, but give refuge and feed about 95% of the growing population of the area (Gao et al., 2004; Chu et al., 2005).

Direct precipitation to the oases is usually greater than to the neighbouring Badain Jaran and Tengger ~~deserts~~ Deserts (e.g., 120-170 vs. 40-60 kg m^{-2} yr^{-1}; Table 1; Fig. 1). However, this amount is simply too small to support vegetation growth (Bourque and Hassan, 2009), when localised rates of potential evaporation can regularly exceed 2,000 kg m^{-2} yr^{-1} (Ding and Zhang, 2004; Zhang et al., 2008). A significant source of water to the oases is the generation of meltwater in the Qilian Mountains. The meltwater usually flows during the spring-to-summer warming of the mountain glaciers and previous winter's snow cover (Ji et al., 2006). Glacial meltwater currently accounts for about 22% of the total direct supply of inland river water in northwest China, in general (Lu et al., 2005), and < 9% in the Hexi Corridor (Wang et al., 2009). An equally important source of water to the oases is orographic precipitation formed during the spring-fall period of each year (Zhu et al., 2004). Orographic precipitation is formed when air is forced to rise as a result of its interaction with major mountain barriers (Roe, 2005). Isotopic

studies by Ma et al. (2009) confirm the importance of in-mountain production of precipitation and ice- and snow-thawed water in recharging the lowland oases of the area.

<Table 1>

Formatted: Font: Bold

Formatted: Centered

Long term mean recharge in low-lying areas north of the Qinghai-Tibet Plateau (Fig. 1) is assessed to be about 0.9-2.5 kg m^{-2} yr^{-1} (~1-2% of mean annual total precipitation) based on chloride mass-balance and isotopic assessments (Ma et al., 2008; Gates et al., 2008a, 2008b; Ma et al., 2009), indicating that most of the surface and shallow subsurface water generated in the mountains and flowing to the oases is eventually lost to the atmosphere as a result of evaporation. Lack of recharge of groundwater and excessive extraction of the resource for agricultural and other domestic uses has led to salinisation and desertification of the land surface in westcentral Gansu (Zong et al., 2011; Aarnoudse et al., 2012; Currell et al., 2012).

All of these studies and others available in the scientific literature (e.g., Kang et al., 1999; Gates et al., 2008a; Huo et al., 2008; Li et al., 2008; Jia et al., 2010; Ma et al., 2009; Pang et al., 2011; Zhuang et al., 2011; Ma et al., 2013) make reference to the importance of orographic rainout and the role of oasis vegetation in supporting the water cycle in the Hexi Corridor. However, none of these studies explicitly connects in-mountain production of precipitation to the seasonal evolution of oasis vegetation.

Non-geochemical assessments of regional water fluxes are complicated by the scarcity of land and climate data in arid regions of the world. In general, arid and mountainous regions of the world, including northwest China, have few to no monitoring stations. Pilgrim et al. (1988) found that the effective density of hydrometric stations in an arid region of Australia is one

114 station per 10,000 km^2, compared to one station per 2,300 km^2 overall. Quality of data is also
115 compromised in arid regions, due to difficulties in maintaining the~~se~~ stations.

116 Remote sensing and distributed modelling techniques are often used to supplement our
117 understanding of eco-hydrometeorological processes at large spatial extents (e.g., hundreds of
118 thousands km^2) at resolutions suitable ~~to attending to~~to address issues of sustainable
119 development (< 500 m). Integrating remote sensing data with distributed modelling provides us
120 with an efficient ~~effective~~ way of examining localised eco-hydrometeorological processes
121 without resorting to a few point measurements and potentially imprecise methods of
122 interpolation (Matin and Bourque, 2013a), except possibly in the calibration and confirmation of
123 biophysical surfaces derived from remote sensing-based characterisations of regional fluxes.

124 The objective of this paper is to investigate the relative influence of oasis vegetation on
125 water recycling and the generation of in-mountain precipitation in two large endorheic river
126 basins in northwest China over a 10-year period (i.e., 2000-2009), based partially on a
127 correlational and cause-and-effect examination (by way of convergent cross mapping; Sugihara
128 et al., 2012) of relevant hydrological variables. Spatiotemporal variation in oasis-vegetation
129 coverage and phenology is characterised by a chronological series of monthly Moderate
130 Resolution Imaging Spectroradiometer (MODIS)-based images of enhanced vegetation index
131 (Huete et al., 2002) and landcover-specific thresholds. Hydrological components essential to the
132 study involve existing, independently-developed monthly surfaces of (i) evaporation and
133 precipitation, prepared from remote sensing data (Table 2), and (ii) snowmelt and mountain
134 return flow, generated from distributed hydrological modelling (see Matin and Bourque, 2013a
135 and 2013b; Matin and Bourque, 2015). All surfaces were later validated against field data
136 collected at a limited number of climate and hydrometric stations in the Hexi Corridor.

Formatted: Left

<Table 2>

Identifying ~~causation~~ causality between relevant eco-hydrometeorological variables is an important step towards testing the idea that seasonal evolution of oases vegetation and associated production of water vapour in the lowlands are in fact implicated in the production of precipitation in the Qilian Mountains and return flow to the oases. These back and forth transfers of water (in both its gaseous and liquid state) assure the long term ~~self~~ sustainability of desert oases in northwest China. Disruption in the lowland production of water vapour by affecting vegetation growth and coverage through land conversion could potentially result in irreparable damage to the self-supporting mechanisms of the oases by promoting desertification of the area (Warner, 2004; Bourque and Hassan, 2009).

2 Study area

The study area consists of the Shiyang and Hei River basins in westcentral Gansu Province, northwest China (Fig. 1). The Shiyang River basin is an endorheic river basin (Li et al., 2013a) located in the eastern Hexi Corridor. The Shiyang River originates from the Qilian Mountains and flows about 300-km northeastward (Gao et al., 2006) before terminating in the Minqin-lake district, bordering the Tengger and Badain Jaran ~~deserts~~ Deserts (Li et al., 2007; Fig. 1). The basin area is roughly 49,500 km^2. Elevation in the Shiyang River basin varies from 1,284-5,161 m above mean sea level (a.m.s.l.), with an average elevation of 1,871 m a.m.s.l. The Shiyang River system has eight main branches, including the Xida, Donga, Xiying, Jinta, Zamusi, Huangyang, Gulang, and Dajing Rivers (Li et al., 2013a; Wonderen et al., 2010).

Formatted: Font: Bold
Formatted: Centered
Formatted: Left
Formatted: Left

The Hei River also originates from the Qilian Mountains, northwest of the headwaters of the Shiyang River network, and flows northwestward through the oases and terminates in the Badain Jaran Playa (Akiyama et al., 2007). The Hei River basin, with a land surface area of approximately 128,000 km^2, is the second largest endorheic river basin in northwest China (Gu et al., 2008). The Hei River basin includes the Zhangye sub-basin, with a total land area of about 31,100 km^2. Elevation in the Zhangye sub-basin varies from 1,287-5,045 m a.m.s.l., with an average elevation of 2,679 m a.m.s.l.

Long term average data (1950-2000) show that precipitation and potential evaporation in the deserts are approximately 80-150 kg m^{-2} yr^{-1} and 2,300-2,600 kg m^{-2} yr^{-1}, based on an application of the Penman-Monteith equation (Monteith, 1965). Precipitation increases in the mountains from 300-600 kg m^{-2} yr^{-1}, while potential evaporation decreases to about 700 kg m^{-2} yr^{-1} (Akiyama et al., 2007; Wang and Zhao, 2011; Zang et al., 2012). Most of the precipitation occurs during June to August. About 94% of water delivered from the mountains to lowland oases is through surface runoff. Average annual runoff in the Shiyang River is about 15.8×10^8 m^3 yr^{-1}, whereas in the Hei River it is about 37.7×10^8 m^3 yr^{-1} (Kang et al., 2009).

3 Methods

3.1 Landcover types, zones, and regional sampling

Based on vegetation site preferences (Appendix), the study area was subdivided into four main elevation zones (Fig. 2a), defined by elevations: (i) < 2,500 (oasis plains and foothills; Zone 1); (ii) 2,500-3,300 (low-mountain elevations; Zone 2), (iii) 3,300-3,900 (mid-mountain elevations; Zone 3), and (iv) > 3,900 m a.m.s.l. (high-mountain elevations; Zone 4). Different landcover types in these elevation zones were then identified based on enhanced vegetation index and slope

Formatted: Left

orientation (Table A1, Appendix; Fig. 1). To advance the analysis, within-zone enhanced vegetation index, evaporation, and precipitation were sampled randomly in a geographic information system (for sampling point layout, see Fig. 2a).

<Fig. 2>

Formatted: Font: Bold
Formatted: Centered
Formatted: Left

3.2 Vegetation phenology

Formatted: Left

Land surface phenology refers to the timing of different life-cycle stages of plants (Martinez and Gilabert, 2009). Seasonal changes in land surface phenology is important to understand the relationship between vegetation growth and the hydrological cycle in river basins (Martinez and Gilabert, 2009). Study of land surface phenology is also important to understand the causes of vegetation-growth-pattern changes (Fisher and Mustard, 2007; Myneni et al., 1997). Satellite-based analysis of land surface phenology addresses the development patterns in photosynthetic biomass by means of derived vegetation indices (e.g., Fig. 3a; Ahl et al., 2006) in an area that can potentially support many species. Ground-based analysis of land surface phenology, in contrast, focusses on a single plant species at a time.

<Fig. 3>

Formatted: Font: Bold
Formatted: Centered

Typical measures of phenology are (i) onset of greening, (ii) onset of senescence, (iii) peak development during the growing season, and (iv) length of the growing season (Hudson et al., 2010). Various methods have been adopted to assess phenology from space. Hudson et al. (2010) classified these into four groups, namely (i) threshold-, (ii) derivative-, (iii) smoothing-, and (iv)

model-based methods. Among these methods, the threshold-based method is the simplest and most commonly used (Hudson et al., 2010).

With the threshold-based method, a single value of vegetation index is specified as the threshold. The values of vegetation index are plotted against time of year. The time when the threshold value is passed in the upward direction is identified as the start of the growing period and when the same value is passed in the downward direction, the time is identified as the end of the growing period (Karlsen et al., 2006; e.g., Fig. 3b). Methods of selecting the threshold vary among studies. Some authors use single arbitrary thresholds, e.g., 0.17 (Fischer, 1994), 0.09 (Markon et al., 1995), and 0.099 (Lloyd, 1990), whereas some use threshold specifiers like the long term average (Karlsen et al., 2006) or % peak amplitude of vegetation indices (Jonsson and Eklundh, 2002).

In the current analysis, phenological state and regional coverage is specified by monthly MODIS-based images of enhanced vegetation index (Fig. 3a). Different thresholds were identified for each landcover type (Table A1, Appendix) to determine the onset of greening and senescence in the vegetative cover. Threshold values were generated from spatially-distributed 10-year averages of monthly mean enhanced vegetation index. Zonal averages of mean enhanced vegetation index were calculated for each landcover type for each month of the year. These values were plotted against time to generate separate time-vs.-vegetation index plots for each landcover type. The threshold values were specified at the time when mean enhanced vegetation index had maximum positive curvature when moving in the upward direction (Fig. 3b). Values generated were 0.09 for crops and sparse grass, 0.17 for coniferous forest and meadow, and 0.12 for other vegetation types.

3.3 Onset, cessation, and duration of the precipitation season

Most methods used in establishing the onset and cessation of the precipitation season usually aim to determine the effective planting date of crops (Adejuwon et al., 1990; Adejuwon and Odekunle, 2006; Benoit, 1977; Ilesanmi, 1972). In these methods, the onset and end of the precipitation season is equated to the onset and end of the growing season (Benoit, 1977; Odekunle et al., 2005). These methods do not help clarify the relationship between the onset of the growing and precipitation seasons, when the seasons are not entirely synchronised. Cumulative % precipitation (Ilesanmi, 1972) is the most widely used indicator of the onset and cessation of the precipitation season independent of other climatic and vegetation factors (Adejuwon et al., 1990; Adejuwon and Odekunle, 2006; Odekunle, 2006). In this method, daily % precipitation data are processed to generate five-day means. Using these means, cumulative precipitation is plotted against time of year. On these plots, the point of maximum positive curvature is defined as the onset of the precipitation season, whereas the point of maximum negative curvature is defined as the cessation of the season. Points of onset typically happen at the time when cumulative % precipitation is between 7-8%, while times of cessation are when cumulation reaches about 90% (Ilesanmi, 1972). In our analysis, we apply Ilesanmi's (1972) approach to monthly data. Spatial averages of monthly precipitation calculated for the different elevation zones were used to generate cumulative % precipitation curves for each zone as a function of time of year.

3.4 Correlation and causality

Pearson's correlation describes the statistical co-variation between two variables (Gotelli and Ellison, 2013); it does not address matters of cause-and-effect. Correlation is employed in this

study primarily to establish the strength of association between paired combinations of state variables to help form an initial description of potentially relevant eco-hydrometeorological relationships.

Recent advances in dynamic-systems analysis have resulted in the development of innovative methods for identifying causality in timeseries data (Sugihara et al., 2012). One such method, convergent cross mapping, is a model-free approach that helps identify causality and direction of causality in dynamically-evolving systems. Timeseries variables are considered causally connected if both are derived from the same dynamic system. Convergent cross mapping checks for causation by measuring the extent historical registrations in one variable (i.e., timeseries one) can consistently approximate the state in a second variable (timeseries two). The method is able to provide reliable description of causality even in the presence of system feedback and confoundedness (Sugihara et al., 2012). Moreover, convergent cross mapping involves convergence, an important methodological attribute that differentiates causation from ordinary correlation (Maher and Hernandez, 2015). In general, non-causal relationships are illustrated as flat curves of predictive skill, based on calculations of Pearson's correlation between predictions and actual observations, with respect to variations in timeseries length. Causation is suggested when convergence is present and Pearson's correlation at the point of convergence is greater than zero. It is always possible to get bi-directional convergence when variables are strongly forced by an external third variable, resulting in synchrony between variables being assessed. Synchrony should be tested for convergent cross mapping to determine bi-directional pairing (Sugihara et al., 2012; Clark et al., ~~2014~~2015). When synchrony exists, it can sometimes be minimised by processing the "first difference" of cross-correlated variables by subtracting previous observations (at time *t-1*) from current observations (at *t*) in the original

timeseries prior to performing the analysis (Granger and Newbold, 1974). In this paper, we use convergent cross mapping to assess the direction and strength of causality between (i) enhanced vegetation index and evaporation in the oases, and (ii) evaporation in the oases and production of precipitation in the high mountains, most notably in Zone 4 (Fig. 2a).

4 Results and Discussion

4.1 Vegetation development timing

Onset of greening occurs mostly in early April, except in some parts of the study area, where the growing season is slightly advanced (i.e., initiating in late March; Fig. 3). In the forest and meadow areas of the mountains, the growing season commences in May, and in some parts, in June. Early changes in vegetation development patterns (changes in monthly enhanced vegetation index) in the upper mountains of the river basins may occur as a result of localised melting of the snowpack during a time when atmospheric temperatures are favourable for plant growth. Vegetation growth reaches its peak in July-August and dies back in all areas of the study area in November, except in the high mountains of the Hei River basin, where vegetation senescence is observed to occur in October.

4.2 Oasis enhanced vegetation index development vs. evaporation

Average regional evaporation (Fig. 4) as a function of average enhanced vegetation index (Fig. 3) over the growing season (April through October) suggest that regional evaporation has strongest positive correlation with vegetation in the oases, with very high r^2-values when crops and dense grass were considered; i.e., 0.85, 0.83 and 0.84, 0.73 for the Shiyang and Hei River

basins, respectively. Correlation with landcover types in the mountains is also present, but at a much reduced level (Table 3).

<Fig. 4>

<Table 3>

Convergent cross mapping of oases timeseries data of enhanced vegetation index with evaporation indicates feedback (bi-directional causality) between the two variables (p-values < 0.05; Fig. 5a and 5b), with plant-mediated evaporation providing marginally stronger control over plant growth, i.e., Pearson's correlation coefficient at the point of convergence (at the largest record length) for "B causes A" is greater than that for "A causes B", where A represents changes in enhanced vegetation index and B, changes in oasis evaporation (Fig. 5b). ~~Fig.~~Figures 5a and 5b give the results with respect to the original, unprocessed timeseries data and "first differencing" of the original data, respectively. Both are provided because convergence illustrated in Fig. 5a does not completely guarantee bi-directional causality, because of possibility of synchrony between the two variables.

<Fig. 5>

Bi-directional causality between the seasonal evolution of oasis vegetation and evaporation (transpiration) is not surprising, as the transpiration process is central to moving water-soluble nutrients vital to plant growth from the soil to the various parts of the plant

Formatted: Font: Bold
Formatted: Centered
Formatted: Font: Bold
Formatted: Font: Bold
Formatted: Centered

(Kimmins, 1997) and in support of plant biochemical processes (~1-5% of available water). As plants produce leaf biomass, increasing leaf surface area (and, thus, enhanced vegetation index), transpirational fluxes become stronger providing that solar irradiation, atmospheric conditions (e.g., temperature, humidity, and wind speeds), and soil water are not limiting ~~factors~~. Elevated transpiration rates also help cool vegetation in hot environments (e.g., Fig. 2b), promoting improved growing conditions for the vegetation during the hotter part of the growing season.

4.3 Evaporation in the oases vs. precipitation in the high mountains

The precipitation season for the most part starts in late April to early May (Fig. 6a through 6c) and ends in September with nominal interannual variation in timing. Greatest interannual variation in cumulative % amounts is observed to occur in the lowlands (Zone 1) of both river basins, and the least in the mountains (e.g., Zones 3 and 4; Fig. 6b). Interannual variation in the lowlands is most likely associated with the convective nature of locally-generated precipitation (Zhang et al., 2010).

<Fig. 6>

Formatted: Font: Bold

Formatted: Centered

Pairwise correlations within individual river basins reveal that within-zone vegetation is weakly associated to precipitation generated locally (i.e., within the same zone), but precipitation in the mountains has the strongest correlation with vegetation (i.e., crops and grasses) and evaporation in the oases (Table 4). These correlations become particularly strong in the high mountains (i.e., Zone 4). This measured increase in correlative strength is expected as the monthly precipitation signal becomes stronger and more continuous with upward elevation~~;~~ as

the impact of a variable lifting condensation level (Fig. 6d) and localised (within-zone) contribution of evaporation becomes less effective pronounced at higher elevations (Fig. 6d). The lifting condensation level of moistened air (i.e., the level rising air becomes saturated) defines the cloud-base height and the lowest level that precipitation can form from orographic (adiabatic) lifting. The lifting condensation level varies with relative humidity of the air prior to its vertical displacement at the base of the mountain barrier, resulting in temporal variation in the cloud-base elevation (Fig. 6d) and the portion of the mountain range affected by orographic precipitation (Bourque and Hassan, 2009).

<Table 4>

Formatted: Font: Bold

Formatted: Centered

Convergent cross mapping of timeseries data of oasis evaporation with precipitation in the high mountains of both river basins also correctly points to bi-directional causality (feedback) between the two variables (p-values < 0.05 for all instances, except one; Fig. 5c and 5d), with the lowland production of water vapour providing the stronger control between the two variables (Fig. 5d). Rainwater generated in the high mountains eventually returns to the oases during the same growing season. This source of water is, in turn, used to promote continued vegetation growth in the oases and the production of water vapour during the growing period (see Section 4.2), intensifying the production of precipitation in the mountains. During the non-growing part of the year (i.e., November through February of the following year), in-mountain precipitation is observed to be consistently lower than the rest of the year (Fig. 6a and 6c). This is mainly due to the fact that vegetation growth (Fig. 3), evaporation (Fig. 4), and water vapour content at the base of the mountains (Fig. 6e) are their smallest and least effective during this

time of year. ~~This relationship~~ This trend was also observed in an earlier study examining the level of snow (as a passive tracer) and coverage in the mountains in the same area during the non-growing part of the year ~~addressed~~ replicated in simulations~~by~~ with process models and assessed ~~results from~~ as part of an analysis of remote-sensing optical (MODIS) and passive microwave data (e.g., Advanced Microwave Scanning Radiometer-Earth Observing System~~) data~~ ~~(~~; Bourque and Matin, 2012; Matin and Bourque, 2013a).

Winds associated with orographic lifting generally arise from the northwest to east-southeast sector, 61.3 and 48.1% of the time during the growing season for the Shiyang and Hei River basins, respectively (Fig. 7a). In the Hei River basin, winds from the northwest (most frequent wind direction within the northwest to east-southeast sector) actually transport water vapour to the mountains of the Shiyang River basin (Fig. 7b, lower diagram) causing precipitation levels to be slightly greater in the Shiyang River basin than in the Hei River basin (Table 3). The Hei River basin may at times receive water vapour from the Shiyang River basin, but the possibility of that occurring is significantly reduced, given that winds from the east to east-northeast sector are quite uncommon (< 5% of the time: Fig. 7a) and mountains in the Shiyang River basin may cause water vapour content of the affected air to be reduced by orographic lifting. Small oases west of Zhangye Oasis (e.g., Jinta and Jiuguan Oases) are not geographically in position for the prevailing winds of the area (i.e., northwest to north-northwest winds) to contribute significant amounts of water vapour to the upper-portion of the Hei River basin.

<Fig. 7>

Formatted: Font: Bold

Formatted: Centered

Formatted: Font: Bold

Asynchrony in the start of the oasis growing and in-mountain precipitation seasons (Fig. 3 and 6), suggests that the amount of water vapour sufficient to trigger the precipitation season in the Qilian Mountains requires on average at least one month of active plant growth to ensue (Fig. 8). Commencement of the growing season in the oases is governed to a large extent by the warming atmosphere during early spring (i.e., with the accrual of sufficient growing degree-days) and accessibility to adequate soil water. ~~The~~ A vital source of water to support initial vegetation growth in the oases is surface water generated by snowmelt in the plain and lower-mountain positions (< 3,300 m a.m.s.l.) during the March-April period of each year (Fig. 8). Meltwater production in the lower mountains of both river basins is about the same (i.e., 250 × 10^6 m^3 in the Shiyang vs. 223 × 10^6 m^3 in the Hei River basins, respectively), whereas it is substantially greater in the mid- to high-mountain portions of the Hei River basin (i.e., 299 × 10^6 m^3 in the Shiyang vs. 1,129 × 10^6 m^3 in the Hei River basin), as a result of differences in respective land-surface ~~areas~~ area at high elevations, i.e., 2,979 vs. 10,328 km^2 for the Shiyang and Hei River basins. Delivery of this snowmelt water to the oases occurs until August, when air temperatures in the high mountains begin to decline (Fig. 8c~~,~~ and 8d).

<Fig. 8>

Formatted: Font: Bold

Formatted: Centered

4.4 Zone-specific water yield

~~In the oases, water vapour production by crops and grasses exceed locally generated precipitation.~~ Comparisons between annual cumulative water volumes associated with the sum of rainfall and snowmelt with those of evaporation for corresponding elevation zones and for the total river basin show that annual water volumes associated with evaporation (E) exceeds those

of rainfall (P) + snowmelt (S) in the oases (i.e., P + S – E < ~~0.0~~0 and E/(P+S) > 100%), with the opposite being true in the mountains (i.e., P + S – E > ~~0.0~~0 and E/(P+S) < 100%; Table 5). ~~Differences~~ Volume ratios in the mountains ~~([~~i.e., E/(P+S)~~P + S – E)~~] tend to ~~increase~~ decrease with increased elevation because of corresponding increases in rainfall and snowmelt (to a certain elevation threshold; see Matin and Bourque, 2015) and decreases in evaporation. Total water volume associated with rainfall and snowmelt collectively is about equal to that of evaporation at the river-basin level, i.e., 90% and 89% for the Shiyang and Hei River basins, respectively (Table 5). ~~This~~ Given the importance of in-mountain production of precipitation to the local hydrological cycle, this suggests that ~~the bulk~~a significant ~~of~~fraction of precipitation ~~water~~ originating ~~from~~ in the mountains and returning to the oasis as surface and shallow subsurface runoff ~~(~90%)~~ is ~~eventually~~ likely to return~~ed~~ to the mountains as evaporated water. Given the right wind directions (Fig. 7), ~~Water~~ water vapour generated by the oasis can travel across ~~the~~ boundaries of river basins ~~as illustrated earlier~~ and contribute to the production of precipitation in the mountains of neighbouring basins. ~~,~~ Once ~~but once~~ deposited, surface water is mostly confined to the basin that precipitation was formed in. ~~This~~ These results and all other results in preceding sections are consistent with a hydrologically-closed system.

<Table 5>

Formatted: Font: Bold

Formatted: Centered

Recycling ratios for the study area are expected to be significantly greater that those reported in van der Ent et al.'s (2010) global moisture-recycling analysis (i.e., < 5% for northwest China, based on their Fig. 5, contrasted with potentially as high as 90%, for this study). Since regional recycling ratios are scale-dependent (van der Ent et al., 2010), these

differences ~~may~~ are not to be unexpected. The grid-cell size (scale) used in the current study (250 m × 250 m) may have allowed for the capture of ~~detail~~ information that was effectively invisible to the global analysis, based on a 1.5^{o} latitude × 1.5^{o} longitude scale (van der Ent et al., 2010).

5 Conclusions

This paper examines ~~analyses~~ the interdependencies between different components of the hydrological cycle of the Shiyang and Hei River study basins. By correlating and cross-mapping precipitation, evaporation, and vegetation within different elevation zones of the river basins, the analysis reveals that oasis vegetation has an important role in sustaining the water cycle in both river basins. Oasis vegetation is dependent on surface water flowing to the region from mountain surface and shallow-subsurface sources. Surface runoff is generated from the precipitation falling in the adjoining mountains. Correlation analysis shows that in-mountain-generated precipitation is strongly correlated to the state of oasis vegetation (r^2 = 0.65 and 0.85 for the Shiyang and Hei River basin, respectively) and water vapour generated by evaporation (r^2 = 0.57 and 0.77). Convergent cross mapping of related timeseries revealed bi-directional causality (feedback) between paired variables (i.e., enhanced vegetation index vs. evaporation in the oases and evaporation in the oases vs. production of precipitation in the high mountains). Comparisons between the onset of vegetation development and the precipitation season shows that the growing season precedes the precipitation season in the oases by, on average, one month. This suggests that vegetation growth in the oases, through the production of water vapour, provides an initial triggering of the precipitation season in the mountains. Onset of vegetation development in the oases is supported by atmospheric warming (accumulation of sufficient

growing degree-days) and the generation of snowmelt in the mountains in March through April. Analysis of annual total water volume involved at the basin-level seems to ~~indicate~~ suggest that ~~rainfall and snowmelt together, integrated across the entire river basins, accounts for about 90% of~~ water vapour ~~transported to the mountains, as a result of~~generated locally (within basin) ~~evaporation in the oases~~ coincides with about 90% of precipitation (direct rainfall + snowmelt) produced in the same basin. Isotopic studies carried out at the appropriate eco-hydrometeorological scale (oasis-mountain scale) could help corroborate this ecologically-significant finding.

Appendix A: Landcover types

Vegetation distribution in the study area (Fig. 1 of the main text) has a unique preferential association with elevation, slope, and slope direction (Jin et al., 2008). For instance, < 2,500 m a.m.s.l., the growing environment for spring wheat (prominent crop grown in the study area) and dense grass is limited to the desert oases (Zhao et al., 2005; Fig. 1). North-facing slopes of the Qilian Mountains support alpine meadow at elevations between 2,500 to 3,300 m a.m.s.l. At elevations > 3,300 m a.m.s.l., deciduous shrubs represent the most dominant vegetation type. Isolated patches of conifer forests in the Qilian Mountains (mostly ~~involving~~ consisting of Qinghai spruce, *Picea crassifolia*) are found to grow best at elevations between 2,500 m to 3,300 m a.m.s.l. (Carpenter, 2001). Seasonal vegetation density and growth vary as a function of both vegetation type and elevation.

The MODIS-based annual global landcover map currently available, as of 2012, is produced from seven spectral maps, bi-directional reflectance distribution ~~function (BRDF) adjusted~~function adjusted reflectance, land surface temperature ~~(T_s)~~, enhanced vegetation index,

and an application of supervised classification using ground data from 1860 field sites (Friedl et al., 2010). Assessments of the product have shown that this map is not entirely realistic for zones of steep transition, particularly in mountainous areas (Liang and Gong, 2010). Improved landcover definition at regional or local scales with supervised classification usually involves much greater amounts of ground data that are normally available for most regions. Recently, decision-tree based classifications have been applied to remote sensing data and has been shown to produce better results than other classification systems, based on maximum likelihood or unsupervised clustering and labelling (Friedl and Brodley, 1997). One benefit of decision-tree based classification is that it is able to use local knowledge of vegetation characteristics together with other pertinent information, such as terrain characteristics, in its evaluation. In the current study, chronological-sequences of MODIS-based enhanced vegetation index and digital terrain information of the study area (e.g., slope orientation, elevation) are used to classify landcover with a decision-tree classifier.

One landcover map was generated for each year during the 2000-2009 period using classification thresholds summarised in Table A1. From these maps, a composite landcover map was then created based on a pixel-level assessment of the most common landcover type of the nine possible types (Table A1; Fig. 1) during the ten-year period.

503

504 **Table A1.** Landcover type definition as a function of elevation zone, enhanced vegetation index
505 (EVI), and slope orientation.

Zone[a]	Landcover Type	Classification Thresholds
1	Desert	Maximum growing-season EVI < 0.113
	Crop	Maximum growing-season EVI > 0.27 and minimum growing-season EVI < 0.113
	Dense grass	Maximum growing-season EVI > 0.27, and minimum growing season EVI > 0.113
	Sparse grass and/or shrub	Maximum growing-season EVI between 0.113-0.27 and mean growing season EVI > 0.113
	Bare ground	Maximum growing-season EVI between 0.113-0.27 and mean growing season EVI < 0.113
2	Alpine meadow	Maximum growing-season EVI > 0.27 and on north-facing slopes
	Coniferous forest	Maximum growing-season EVI > 0.27, but not on north-facing slopes
	Sparse grass and/or shrub	Maximum growing season EVI between 0.113-0.27
	Bare ground	Maximum growing-season EVI < 0.113
3	Deciduous shrub	Maximum growing-season EVI > 0.27
	Bare ground	Maximum growing-season EVI < 0.27
4	Sparse shrub	Maximum growing-season EVI > 0.113
	Snow and/or ice	Maximum growing-season EVI < 0.113

506 [a] Zones are classified according to elevation bands: < 2,500 m (Zone 1); 2,500-3,300 m (Zone 2); 3,300-3,900 m (Zone 3); and >
507 3,900 m a.m.s.l. (Zone 4).
508

Formatted: Font: 9 pt

Formatted: Font: 7 pt

509 **Acknowledgements**

510 This study was jointly funded by: (i) Lanzhou Regional Climate Centre of the Gansu Provincial
511 Meteorological Bureau (GMB), Lanzhou, China (National Natural Science Foundation of China,
512 Grant Number 40830957), (ii) the Natural Science and Engineering Research Council of Canada
513 (NSERC) through a Discovery Grant to CPAB; and (iii) the Faculty of Forestry and
514 Environmental Management, University of New Brunswick, New Brunswick, Canada with its
515 financial support of MAM in the form of graduate-student research and teaching assistantships.
516 We would like to acknowledge the USA National Aeronautics and Space Administration and
517 Geological Survey for providing MODIS and SRTM v. 4 DEM data free of charge. Finally, we
518 are grateful for the suggestions provided by two reviewers of the initial manuscript.

519 **References**

520 Aarnoudse, E., Bluemling, B., Wester, P., and Qu, W.: The role of collective groundwater
521 institutions in the implementation of direct groundwater regulation measures in Minqin
522 County, China. Hydrogeol. J., 20, 7, 1213-1221, http://dx.doi.org/10.1007/s10040-012-
523 0873-z, 2012.
524 Adejuwon, J. O., Balogun, E. E., and Adejuwon, S. A.: On the annual and seasonal patterns of
525 rainfall fluctuations in sub-saharan West Africa. Int. J. Climatol., 10, 8, 839-848,
526 http://dx.doi.org/10.1002/joc.3370100806, 1990.
527 Adejuwon, J. O., and Odekunle, T. O.: Variability and the severity of the "Little Dry Season" in
528 southwestern Nigeria. J. Climate, 19, 3, 483-493, http://dx.doi.org/10.1175/jcli3642.1,
529 2006.
530 Aguado, E., and Burt, J. E.: Undertstanding Weather and Climate, 6th ed. Pearson Education Inc.,
531 NY, 552 pp, 2013.
532 Ahl, D. E., Gower, S. T., Burrows, S. N., Shabanov, N. V., Myneni, R. B., and Knyazikhin, Y.:
533 Monitoring spring canopy phenology of a deciduous broadleaf forest using MODIS.
534 Remote Sens. Environ., 104, 1, 88-95, http://dx.doi.org/10.1016/j.rse.2006.05.003, 2006.
535 Akiyama, T., Sakai, A., Yamazaki, Y., Wang, G., Fujita, K., Nakawo, M., Kubota, J., and
536 Konagaya, Y.: Surfacewater-groundwater interaction in the Heihe River Basin,
537 Northwest China. Bull. Glaciol. Res., 24, 87-94, 2007.
538 Benoit, P.: The start of the growing season in Northern Nigeria. Agr. Meteorol., 18, 2, 91-99,
539 http://dx.doi.org/http://dx.doi.org/10.1016/0002-1571(77)90042-5, 1977.
540 Bourque, C. P.-A., and Hassan, Q. K.: Vegetation control in the long-term self-stabilization of
541 the Liangzhou Oasis of the upper Shiyang River watershed of westcentral Gansu,
542 Northwest China. Earth Interact., 13, 1-22, http://dx.doi.org/10.1175/2009ei286.1, 2009.
543 Bourque, C. P.-A., and Matin, M. A.: Seasonal snow cover in the Qilian Mountains of Northwest
544 China: Its dependence on oasis seasonal evolution and lowland production of water
545 vapour. J. Hydrol., 454-455, 141-151, 2012.
546 Carpenter, C.: Montane grasslands and shrublands,
547 http://www.worldwildlife.org/science/wildfinder/profiles/pa1015.html, 2001.
548 CGIAR-CSI: SRTM 90-m digital elevation data, http://srtm.csi.cgiar.org/, 2008.

549 Chu, P. C., Lu, S., and Chen, Y.: A numerical modeling study on desert oasis self-supporting
550 mechanisms. J. Hydrol., 312, 256-276, 2005.
551 Clark, A. T., Ye, H., Isbell, F., Deyle, E. R., Cowles, J., Tilman, G. D., and Sugihara, G.: Spatial
552 'convergent cross mapping' to detect causal relationships from short time-series. Ecology,
553 96, 1174-1181, http://dx.doi.org/10.1890/14-1479.1, ~~2014~~2015.
554 Currell, M. J., Han, D. M., Chen, Z. Y., and Cartwright, I.: Sustainability of groundwater usage
555 in northern China: dependence on palaeowaters and effects on water quality, quantity and
556 ecosystem health. Hydrol. Process., 26, 26, 4050-4066, http://dx.doi.org/Doi
557 10.1002/Hyp.9208, 2012.
558 Davidson, A., and Wang, S. S.: Spatiotemporal variations in land surface albedo across Canada
559 from MODIS observations. Can. J. Remote Sens., 31, 5, 377-390, 2005.
560 Ding, H., and Zhang, J.: Relationships between sustainable development and water resources in
561 arid oases area - an example of Hexi Corridor. J. Arid Land Resour. Environ., 18, 50-55,
562 2004.
563 Fischer, A.: A model for the seaonal-variations of vegetation indexes in coarse resolution data
564 and its inversion to extract crop parameters. Remote Sens. Environ., 48, 2, 220-230,
565 http://dx.doi.org/10.1016/0034-4257(94)90143-0, 1994.
566 Fisher, J. I., and Mustard, J. F.: Cross-scalar satellite phenology from ground, Landsat, and
567 MODIS data. Remote Sens. Environ., 109, 3, 261-273,
568 http://dx.doi.org/10.1016/j.rse.2007.01.004, 2007.
569 Friedl, M. A., and Brodley, C. E.: Decision tree classification of land cover from remotely sensed
570 data. Remote Sens. Environ., 61, 3, 399-409, 1997.
571 Friedl, M. A., Sulla-Menashe, D., Tan, B., Schneider, A., Ramankutty, N., Sibley, A., and
572 Huang, X. M.: MODIS collection 5 global land cover: algorithm refinements and
573 characterization of new datasets. Remote Sens. Environ., 114, 1, 168-182,
574 http://dx.doi.org/10.1016/j.rse.2009.08.016, 2010.
575 Gao, B. C., and Kaufman, Y. J.: Water vapor retrievals using moderate resolution imaging
576 spectroradiometer (MODIS) near-infrared channels. J. Geophys. Res.-Atmos., 108, D13,
577 ACH (4-1) - ACH (4-10), http://dx.doi.org/10.1029/2002jd003023, 2003.

578 Gao, Y., Chen, Y., and Lu, S.: Numerical simulation of the critical scale of oasis maintenance
579 and development in the arid regions of northwest China. Adv. Atmos. Sci., 21, 113-124,
580 2004.
581 Gao, Y., Wang, G., Liu, H., Liu, Z., Lin, W., and Wang, J.: Landform effects the distribution and
582 circular mode on groundwater in Shiyang River basin. Beijing, China,
583 http://en.cgs.gov.cn/Achievement/The34thCongress/Evolutional/18050.htm, 2006.
584 Gates, J. B., Edmunds, W. M., Darling, W. G., Ma, J. Z., Pang, Z. H., and Young, A. A.:
585 Conceptual model of recharge to southeastern Badain Jaran Desert groundwater and lakes
586 from environmental tracers. Appl. Geochem., 23, 12, 3519-3534,
587 http://dx.doi.org/10.1016/j.apgeochem.2008.07.019, 2008a.
588 Gates, J. B., Edmunds, W. M., Ma, J. Z., and Scanlon, B. R.: Estimating groundwater recharge in
589 a cold desert environment in northern China using chloride. Hydrogeol. J., 16, 893-910,
590 2008b.
591 Gotelli, N. J., and Ellison, A. M.: A Primer of Ecological Statistics. Sinauer Associates, Inc.,
592 Sunderland, MA, USA, 510 pp, 2004.
593 Granger, C. W. J., and Newbold, P.: Spurious regressions in econometrics. J. Economet., 2, 111-
594 120, 1974.
595 Gu, J., Li, X., and Huang, C. L.: Land cover classification in Heihe River Basin with time series
596 MODIS NDVI data. Fifth International Conference on Fuzzy Systems and Knowledge
597 Discovery, Vol 2, Proceedings, 477-481, http://dx.doi.org/10.1109/Fskd.2008.517, 2008.
598 Huang, L. J., and Wen, X. F.: Temporal variations of atmospheric water vapor δD and $\delta^{18}O$
599 above an arid artificial oasis cropland in the Heihe River Basin. J. Geophys. Res.-Atmos.,
600 119, 11,456-11,476, 2014.
601 Hudson, I. L., Keatley, M. R., Beurs, K., and Henebry, G.: Spatio-temporal statistical methods
602 for modelling land surface phenology. In: Hudson, I. L., and Keatley, M. R. (Ed.),
603 Phenological Research. Springer Netherlands, pp. 177-208, 2010.
604 Huete, A. R., Didan, K., Miura, T., Rodriguez, E. P., Gao, X., and Fereira, L. G.: Overview of
605 the radiometric and biophysical performance of the MODIS vegetation indices. Remote
606 Sens. Environ., 83, 1-2, 195-213, http://dx.doi.org/10.1016/S0034-4257(02)00096-2,
607 2002.

608 Huete, A. R., Litu, H. Q., Batchily, K., and Leeuwen, W. V.: A comparison of vegetation indices
609 over a global set of TM images for EOS-MODIS. Remote Sens. Environ., 59, 3, 440-451,
610 http://dx.doi.org/10.1016/S0034-4257(96)00112-5, 1997.
611 Huo, Z. L., Feng, S. Y., Kang, S. Z., Li, W. C., and Chen, S. J.: Effect of climate changes and
612 water-related human activities on annual stream flows of the Shiyang river basin in and
613 North-West China. Hydrol. Process., 22, 16, 3155-3167,
614 http://dx.doi.org/10.1002/Hyp.6900, 2008.
615 Ilesanmi, O. O.: Empirical formulation of onset, advance, and retreat of rainfall in Nigeria. J.
616 Trop. Geogr., 34, 17-24, 1972.
617 Ji, X. B., Kang, E. S., Chen, R. S., Zhao, W. Z., Zhang, Z. H., and Jin, B. W.: The impact of the
618 development of water resources on environment in arid inland river basins of Hexi
619 region, Northwestern China. Environ. Geol., 50, 6, 793-801,
620 http://dx.doi.org/10.1007/s00254-006-0251-z, 2006.
621 Jia, L., Shang, H., and Menenti, M.: Vegetation response to upstream water yield in the Heihe
622 river by time series analysis of MODIS data. Hydrol. Earth Syst. Sci. Discuss., 7, 4,
623 4177-4218, http://dx.doi.org/10.5194/hessd-7-4177-2010, 2010.
624 Jin, X. M., Zhang, Y. K., Schaepman, M. E., Clevers, J. G. P. W., and Su, Z.: Impact of elevation
625 and aspect on the spatial distribution of vegetation in the qilian mountain area with
626 remote sensing data. The International Archives of the Photogrammetry, Remote Sensing
627 and Spatial Information Sciences, XXXVII, Part B7, 2008.
628 Jonsson, P., and Eklundh, L.: Seasonality extraction by function fitting to time-series of satellite
629 sensor data. IEEE Transactions on Geoscience and Remote Sensing, 40, 8, 1824-1832,
630 http://dx.doi.org/10.1109/Tgrs.2002.802519, 2002.
631 Kang, E. S., Cheng, G. D., Lan, Y. C., and Jin, H. J.: A model for simulating the response of
632 runoff from the mountainous watersheds of inland river basins in the arid area of
633 northwest China to climatic changes. Sci. China Series D-Earth Sci., 42, 52-63,
634 http://dx.doi.org/10.1007/Bf02878853, 1999.
635 Kang, S. Z., Su, X. L., Tong, L., Shi, P. Z., Yang, X. Y., Abe, Y. K., Du, T. S., Shen, Q. L., and
636 Zhang, J. H.: The impacts of human activities on the water-land environment of the
637 Shiyang River basin, an arid region in northwest China. Hydrol. Sci. J., 49, 3, 413-427,
638 http://dx.doi.org/10.1623/hysj.49.3.413.54347, 2009.

639 Karlsen, S. R., Elvebakk, A., Hogda, K. A., and Johansen, B.: Satellite-based mapping of the
640 growing season and bioclimatic zones in Fennoscandia. Glob. Ecol. Biogeogr., 15, 4,
641 416-430, http://dx.doi.org/10.1111/j.1466-822x.2006.00234.x, 2006.
642 Kimmins, J. P.: Forest Ecology: A Foundation for Sustainable Management. Prentice Hall, NJ,
643 596 pp, 1997.
644 Kaufman, Y. J., and Gao, B. C.: Remote sensing of water vapor in the near IR from
645 EOS/MODIS. IEEE Transactions on Geoscience and Remote Sensing, 30, 5, 871-884,
646 http://dx.doi.org/10.1109/36.175321, 1992.
647 Kent-Corson, M. L., Ritts, B. D., Zhuang, G. S., Bovet, P. M., Graham, S. A., and Chamberlain,
648 C. P.: Stable isotopic constraints on the tectonic, topographic, and climatic evolution of
649 the northern margin of the Tibetan Plateau. Earth Planet. Sci. Lett., 282, 158-166, 2009.
650 Li, F., Zhu, G., and Guo, C.: Shiyang River ecosystem problems and countermeasures. Agr. Sci.,
651 4, 2, 72-78, http://dx.doi.org/10.4236/as.2013.42012, 2013a.
652 Li, X., Cheng, G., Liu, S., Xiao, Q., Ma, M., Jin, R., Che, T., Liu, Q., Wang, W., Qi, Y., Wen, J.,
653 Li, H., Zhu, G., Guo, J., Ran, Y., Wang, S., Zhu, Z., Zhou, J., Hu, X., and Xu, Z.: Heihe
654 watershed allied telemetry experimental research (HiWATER): Scientific objectives and
655 experimental design. Bull. Amer. Meteorol. Soc., http://dx.doi.org/10.1175/bams-d-12-
656 00154, 2013b.
657 Li, X. Y., Xiao, D. N., He, X. Y., Chen, W., and Song, D. M.: Factors associated with farmland
658 area changes in arid regions: a case study of the Shiyang River Basin, Northwestern
659 China. Front. Ecol. Environ., 5, 3, 139-144, http://dx.doi.org/10.1890/1540-
660 9295(2007)5[139:Fawfac]2.0.Co;2, 2007.
661 Li, Z. L., Xu, Z. X., Li, J. Y., and Li, Z. J.: Shift trend and step changes for runoff time series in
662 the Shiyang River Basin, Northwest China. Hydrol. Process., 22, 23, 4639-4646,
663 http://dx.doi.org/10.1002/Hyp.7127, 2008.
664 Liang, L., and Gong, P.: An assessment of MODIS collection 5 global land cover product for
665 biological conservation studies. Eighteen International Conference on Geoinformatics,
666 2010.
667 Lloyd, D.: A phenological classification of terrestrial vegetation cover using shortwave
668 vegetation index imagery. Int. J. Remote Sens., 11, 12, 2269-2279, 1990.

669 Lopes, A. M. G.: WindStation - a software for the simulation of atmospheric flows over complex
670 topography. Environ. Model. Softw., 18, 81-96. doi: 10.1016/s1364-8152(02)00024-5,
671 2003.
672 Lu, A., Ding, Y., Pang, H., Yuan, L., and He, Y.: Impact of global warming on water resource in
673 arid area of northwest China. J. Mt. Sci., 2, 313-318, 2005.
674 Ma, J. Z., Chen, L. H., He, J. H., Zhang, Y. R., Li, X. H., and Edmunds, W. M.: Trends and
675 periodicities in observed temperature, precipitation and runoff in a desert catchment: case
676 study for the Shiyang River Basin in Northwestern China. Water Environ. J., 27, 1, 86-
677 98, http://dx.doi.org/10.1111/j.1747-6593.2012.00329.x, 2013.
678 Ma, J. Z., Ding, Z. Y., Edmunds, W. M., Gates, J. B., and Huang, T. M.: Limits to recharge of
679 groundwater from Tibetan plateau to the Gobi desert, implications for water management
680 in the mountain front. J. Hydrol. 364, 128-141, 2009.
681 Ma, J. Z., Ding, Z. Y., Gates, J. B., and Su, Y.: Chloride and the environmental isotopes as the
682 indicators of the groundwater recharge in the Gobi Desert, northwest China. Environ.
683 Geol., 55, 1407-1419, 2008.
684 Ma, J. Z., Zhang, P., Zhu, G. F., Wang, Y. Q., Edmunds, W. M., Ding, Z. Y., and He, J. H.: The
685 composition and distribution of chemicals and isotopes in precipitation in the Shiyang
686 River system, northwestern China. J. Hydrol., 436-437, 92-101, 2012.
687 Mahar, M. C., and Hernandez, R. D.: CauseMap: fast inference of causality from complex time
688 series. PeerJ 3:e824; doi:10.7717/peerj.824, 2015.
689 Markon, C. J., Fleming, M. D., and Binnian, E. F.: Characteristics of vegetation phenology over
690 the Alaskan landscape using time-series data. Polar Rec., 31, 177, 179-190, 1995.
691 Martinez, B., and Gilabert, M. A.: Vegetation dynamics from NDVI time series analysis using
692 the wavelet transform. Remote Sens. Environ., 113, 9, 1823-1842,
693 http://dx.doi.org/10.1016/j.rse.2009.04.016, 2009.
694 Matin, M. A., and Bourque, C. P.-A.: Intra- and inter-annual variations in snow-water storage in
695 data sparse desert-mountain regions assessed from remote sensing. Remote Sens.
696 Environ., 139, 18-34, http://dx.doi.org/10.1016/j.rse.2013.07.033, 2013a.
697 Matin, M. A., and Bourque, C. P.-A.: Assessing spatiotemporal variation in actual
698 evapotranspiration for semi-arid watersheds in northwest China: Evaluation of two

complementary-based methods. J. Hydrol., 486, 455-465, http://dx.doi.org/10.1016/j.jhydrol.2013.02.014, 2013b.

Matin M. A., and Bourque, C. P.-A.: Mountain-river runoff components and their role in the seasonal development of desert-oases in northwest China. J. Arid Environ., ~~in review~~122, 1-15, doi: 10.1016/j.jaridenv.2015.05.011, 2015.

Meng, X., Lu, S., Gao, Y., and Guo, J.: Simulated effects of soil moisture on oasis self-maintenance in a surrounding desert environment in Northwest China. Int. J. Climatol., doi:10.1002/joc.4271, 2015.

Meng, X., Lu, S., Zhang, T., Ao, Y., Li, S., Bao, Y., Wen, L., and Luo, S.: Impacts of inhomogeneous landscapes in oasis interior on the oasis self-maintenance mechanism by integrating numerical model with satellite data. Hydrol. Earth Syst. Sci., 16, 3729-3738, 2012.

Meng, X. H., Lu, S. H., Zhang, T. T., Guo, J. X., Gao, Y. H., Bao, Y., Wen, L. J., Luo, S. Q., and Liu, Y. P.: Numerical simulations of the atmospheric and land conditions over the Jinta oasis in northwestern China with satellite-derived land surface parameters. J. Geophys. Res., 114, D06114, 2009.

Meybeck, M.: Global analysis of river systems: from Earth system controls to anthropocene syndromes. Philos. Trans. R. Soc. B-Biol. Sci., 358, 1440, 1935-1955, http://dx.doi.org/10.1098/rstb.2003.1379, 2003.

Meybeck, M., Green, P., and Vorosmarty, C.: A new typology for mountains and other relief classes: An application to global continental water resources and population distribution. Mt. Res. Dev., 21, 1, 34-45, http://dx.doi.org/10.1659/0276-4741(2001)021[0034:Antfma]2.0.Co;2, 2001.

Monteith, J. L.: Evaporation and environment. Sym. Soc. Exp. Biol., 19, 205-34, 1965.

Myneni, R. B., Keeling, C. D., Tucker, C. J., Asrar, G., and Nemani, R. R.: Increased plant growth in the northern high latitudes from 1981 to 1991. Nature, 386, 6626, 698-702, http://dx.doi.org/10.1038/386698a0, 1997.

Odekunle, T. O.: Determining rainy season onset and retreat over Nigeria from precipitation amount and number of rainy days. Theor. Appl. Climatol., 83, 1-4, 193-201, http://dx.doi.org/10.1007/s00704-005-0166-8, 2006.

Formatted: Font: (Default) Times New Roman, 11 pt

Formatted: Font: (Default) Times New Roman, 11 pt

729 Odekunle, T. O., Balogun, E. E., and Ogunkoya, O. O.: On the prediction of rainfall onset and
730 retreat dates in Nigeria. Theor. Appl. Climatol., 81, 1-2, 101-112,
731 http://dx.doi.org/10.1007/s00704-004-0108-x, 2005.
732 Pang, Z. H., Kong, Y. L., Froehlich, K., Huang, T. M., Yuan, L. J., Li, Z. Q., and Wang, F. T.:
733 Processes affecting isotopes in precipitation of an arid region. Tellus, 63B, 352-359,
734 2011.
735 Petitcolin, F., and Vermote, E.: Land surface reflectance, emissivity and temperature from
736 MODIS middle and thermal infrared data. Remote Sens. Environ., 83, 1-2, 112-134,
737 http://dx.doi.org/10.1016/S0034-4257(02)00094-9, 2002.
738 Pilgrim, D. H., Chapman, T. G., and Doran, D. G.: Problems of rainfall-runoff modeling in arid
739 and semiarid regions. Hydrol. Sci. J., 33, 4, 379-400,
740 http://dx.doi.org/10.1080/02626668809491261, 1988.
741 Reuter, H. I., Nelson, A., and Jarvis, A.: An evaluation of void-filling interpolation methods for
742 SRTM data. Int. J. Geogr. Inf. Sci., 21, 9, 983-1008, 2007.
743 Roe, G. H.: Orographic precipitation. Ann. Rev. Earth Planet. Sci., 33, 645-671, 2005.
744 Seeman, S. W., Borbas, E. E., Li, J., Menzel, W. P., and Gumley, L. E.: MODIS atmospheric
745 profile retrieval, algorithm theoritical basis document. ver. 6, Reference Number ATBD-
746 MOD07. Cooperative Institute for Meteorological Satellite Studies, Madison, WI,
747 http://modis.gsfc.nasa.gov/data/atbd/atbd_mod07.pdf, 2006.
748 Shiklomanov, I. A.: World water resources: A new appraisal and assessment for the 21st Century.
749 UNESCO, http://www.ce.utexas.edu/prof/mckinney/ce385d/Papers/Shiklomanov.pdf,
750 1998.
751 Sugihara, G., May, R., Ye, H., Hsieh, C. H., Deyle, E., Fogarty, M., and Munch, S.: Detecting
752 causality in complex ecosystems. Science, 338, 496-500, 2012.
753 van der Ent, R. J., Savenjie, H. H. G., Schaefli, B., and Steele-Dunne, S. C.: Origin and fate of
754 atmospheric moisture over continents. Water Resour. Res., 46, W09525,
755 doi:10.1029/2010WR009127, 2010.
756 Wan, Z., Zhang, Y., Zhang, Q., and Li, Z. L.: Quality assessment and validation of the MODIS
757 global land surface temperature. International J. Remote Sens., 25, 1, 261-274,
758 http://dx.doi.org/10.1080/0143116031000116417, 2004.

759 Wang, J. S., Feng, J. Y., Yang, L. F., Guo, J. Y., and Pu, Z. X.: Runoff-denoted drought index
760 and its relationship to the yields of spring wheat in the arid area of Hexi Corridor,
761 Northwest China. Agr. Water Manage., 96, 4, 666-676,
762 http://dx.doi.org/10.1016/j.agwat.2008.10.008, 2009.
763 Wang, X., and Zhao, C.: Analysis of temporal trends in potential evapotranspiration over Heihe
764 River basin. Presented at the 2011 International Symposium on Water Resource and
765 Environmental Protection (ISWREP), Xi'an, 20-22 May 2011,
766 http://dx.doi.org/10.1109/iswrep.2011.5893130, 2011.
767 Warner, T. T.: Desert Meteorology. Cambridge University Press, Cambridge, NY, 595 pp, 2004.
768 Wen, X. H., Lu, S. H., and Jin, J. M.: Integrating remote sensing data with WRF for improved
769 simulations of oasis effects on local weather processes over an arid region in
770 northwestern China. J. Hydrometeorol., 13, 573-587, 2012.
771 Wonderen, J. V., Moore, D., Wardlaw, R., Zhongjing, W., Litang, H., and Qingling, S.: Water
772 resources and modelling in the Shiyang River Basin, Presented at the BHS Third
773 International Symposium, Managing Consequences of a Changing Global Environment,
774 Newcastle, 2010.
775 Zang, C. F., Liu, J., van der Velde, M., and Kraxner, F.: Assessment of spatial and temporal
776 patterns of green and blue water flows under natural conditions in inland river basins in
777 Northwest China. Hydrol. Earth Syst. Sci., 16, 8, 2859-2870,
778 http://dx.doi.org/10.5194/hess-16-2859-2012, 2012.
779 Zhang, B. Z., Kang, S. Z., Li, F., and Zhang, L.: Comparison of three evapotranspiration models
780 to Bowen ratio energy balance method for a vineyard in an arid desert region of
781 northwest China. Agr. For. Meteorol., 148, 1629-1640, 2008.
782 Zhang, C. J., Bourque, C. P.-A., Sun, L. D., and Hassan, Q. K.: Spatiotemporal modeling of
783 monthly precipitation in the upper Shiyang River watershed in west central Gansu,
784 northwest China. Adv. Atmos. Sci., 27, 1, 185-194, 2010.
785 Zhao, C., Nan, Z., and Cheng, G.: Methods for estimating irrigation needs of spring wheat in the
786 middle Heihe Basin, China. Agr. Water Manage., 75, 1, 54-70,
787 http://dx.doi.org/10.1016/j.agwat.2004.12.003, 2005.

788 Zhu, Y. H., Wu, Y. Q., and Drake, S.: A survey: obstacles and strategies for the development of
789 ground-water resources in arid inland river basins of Western China. J. Arid Environ., 59,
790 2, 351-367, http://dx.doi.org/10.1016/j.jaridenv.2003.12.006, 2004.
791 Zhuang, G. S., Hourigan, J. K., Koch, P. L., Ritts, B. D., and Kent-Corson, M. L.: Isotopic
792 constraints on intensified aridity in Central Asia around 12 Ma. Earth Planet. Sci. Lett.,
793 312, 152-163, 2011.
794 Zong, L., Tedeschi, A., Xue, X., Wang, T., Menenti, M., and Huang, C. H.: Effect of different
795 irrigation water salinities on some yield and quality components of two field-grown
796 Cucurbit species. Turk. J. Agr. For., 35, 3, 297-307, http://dx.doi.org/10.3906/Tar-0908-
797 5, 2011.
798

Figure Captions

Fig. 1. The Shiyang and Hei River basins with distribution of dominant landcover classes, classified with a decision-tree classifier and categorisation thresholds summarised in Table A1 (Appendix). The inset shows the location of the study area along the northeastern flank of the Qinghai-Tibetan Plateau.

Fig. 2. Division of study area according to four elevation zones (a; legend) and mean July air temperature distribution (b) used in the computational fluid-flow dynamics modelling of surface wind velocity (m s^{-1}) and wind direction (^{o} from true North, N). Open circles in (a) give the randomly-selected point-locations where enhanced vegetation index (non-dimensional), evaporation (kg m^{-2} $month^{-1}$), and precipitation (kg m^{-2} $month^{-1}$) were sampled.

Fig. 3. Ten-year average distribution of monthly enhanced vegetation index (EVI $\geq$ 0.15; non-dimensional) according to time of year (a) and spatially-averaged timeseries of monthly EVI over the course of individual years for 2000-2009 (b; shown in different colours). Letters along the x-axis of plots in (b) coincide with month, January (J) through to December (D). Vertical red lines denote the approximate month of the onset (first line) and cessation of the growing season (second line) in the Shiyang and Hei River basins, respectively.

Fig. 4. Ten-year average distribution of monthly evaporation (kg m^{-2} $month^{-1}$) as a function of time of year.

Fig. 5. Predictive-skill curves based on ~~(~~Pearson's correlation coefficients~~)~~ for convergent cross mapping of enhanced vegetation index (EVI) with evaporation in the oases (a, b) and evaporation in the oases with precipitation production in Zone 4 (c, d). Plots (a) and (c)

are based on the original timeseries data, whereas plots (b) and (d) are based on the "first differencing" of the original data. Dotted lines on either side of the predictive-skill curves represent the ± standard error of estimate assessed from bootstrapping ~~with~~ based on 3000 iterations. Convergent cross mapping is based on procedures written in the R-programming language initially developed by Clark et al. (~~2014~~2015). The feature that assures causality in variables is the convergence in the predictive curves as record length increases. Lack of convergence with low Pearson's correlation coefficients indicates lack of causality. The variable with the highest Pearson's correlation coefficients indicates the stronger controlling variable. When curves for both variables are convergent (as is the case here), bi-directional causality and, thus, feedback is indicated. Analyses are based on embedded dimensions and time delays of 4 and 1, respectively (Sugihara et al., 2012).

Formatted: Font: 12 pt, Not Bold

Fig. 6. Ten-year average distribution and timeseries of monthly precipitation (kg m^{-2} $month^{-1}$) according to time of year (a, c) and spatially-averaged cumulative curves of % precipitation over the course of individual years for 2000-2009 (b). Letters along the x-axis of plots in (b) coincide with month, January (J) through to December (D). Vertical red lines denote the approximate time of the onset (first line) and cessation of the precipitation season (second line) in the Shiyang (SR Basin; i-iv) and Hei River basins (HR Basin; v-vii), respectively. Plots (i) through (iv) and (v) through (vii) represent the cumulative % precipitation in the two river basins for Zone 1 through Zone 4. Plots (d) and (e) give the monthly mean lifting condensation level (LCL) and actual water vapour content of air at the base of the Qilian Mountains (i.e., Wuwei City; Table 1) over a different 10-year period (1996-2005). Values of LCL are calculated from $(T_{dry}-T_{dew})/(\Gamma_{dry}-\Gamma_{dew}) \times 1000$ m + elevation at base of Qilian Mountains (i.e., 1534 m at

Wuwei City), where T_{dry} and T_{dew} are the monthly surface dry-bulb and dew-point temperature (both in ^{o}C), and Γ_{dry} and Γ_{dew} are the dry adiabatic and dew-point temperature lapse rates, ~10^{o}C per 1000 m vs. ~2^{o}C per 1000 m, respectively (Warner, 2004: Aguado and Burt, 2013). Vertical dashed lines in (c) to (e) represent the middle of the year.

Fig. 7. Wind direction frequency roses for Zhangye and Liangzhou Oases (a) and calculated wind velocity and direction using a computational fluid-flow dynamics model (b; Lopes, 2003) for prevailing wind directions from the northeast (upper diagrams) and northwest (lower diagram) and July peak near-surface air temperatures (Fig. 2b). Percent values in (a) represent the portion of the time during the growing season that prevailing winds are in directions ~~(within the northwest to east-southeast sector)~~ that will lead to the production of orographic precipitation in the Qilian Mountains (i.e., winds from the northwest to east-southeast directions).

Fig. 8. Ten-year mean monthly snowmelt generated within the different elevation zones (a, b) and mean monthly contribution of rainwater and snowmelt to the monthly river runoff from the Qilian Mountains (based on previous work by Matin and Bourque, 2015) and corresponding monthly enhanced vegetation index for the Shiyang (c) and Hei River basins (d) for the 2000-2009 period.

~~**Fig. 9.** Within-zone average monthly water yield (P + S – E) for 2000-2009. Note the scales of the y-axis for each plot are different.~~

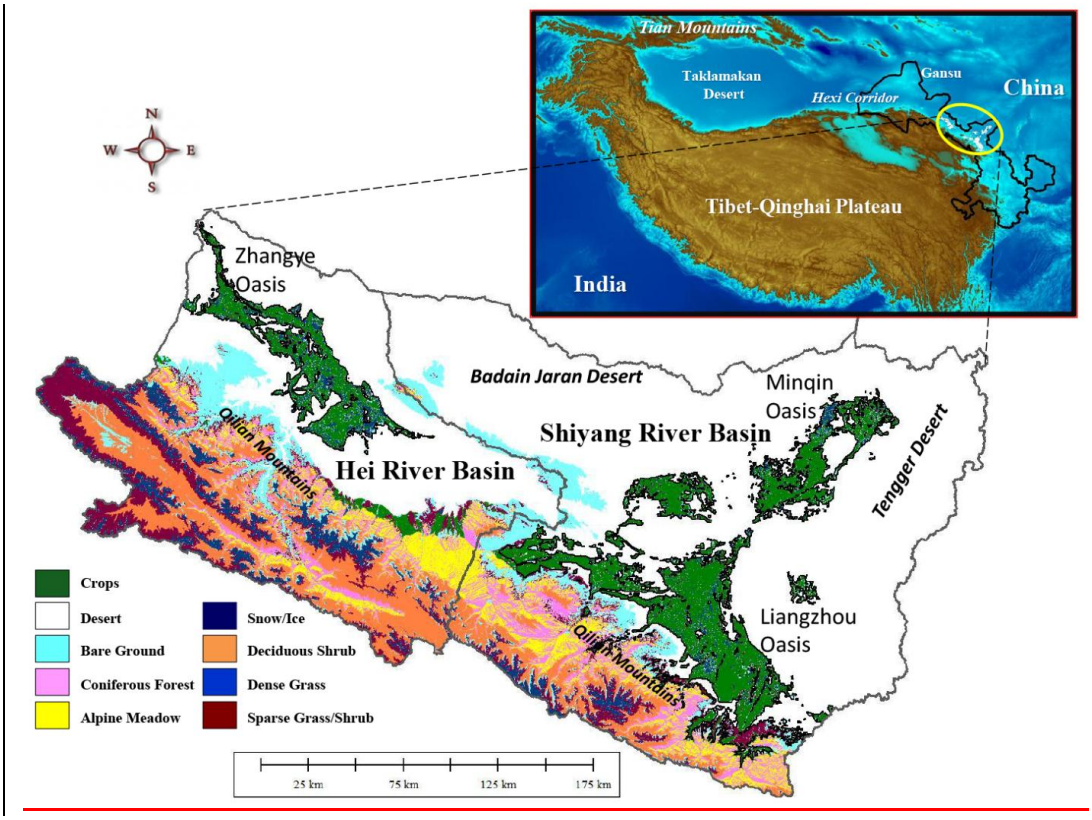
Tian Mountains
Taklamakan Desert
Hexi Corridor
Gansu
China
Tibet-Qinghai Plateau
India
N
W
E
S
Zhangye Oasis
Badain Jaran Desert
Minqin Oasis
Shiyang River Basin
Hei River Basin
Qilian Mountains
Tengger Desert
Liangzhou Oasis
Qilian Mountains
Crops
Desert
Bare Ground
Coniferous Forest
Alpine Meadow
Snow/Ice
Deciduous Shrub
Dense Grass
Sparse Grass/Shrub
25 km
75 km
125 km
175 km

Fig. 1

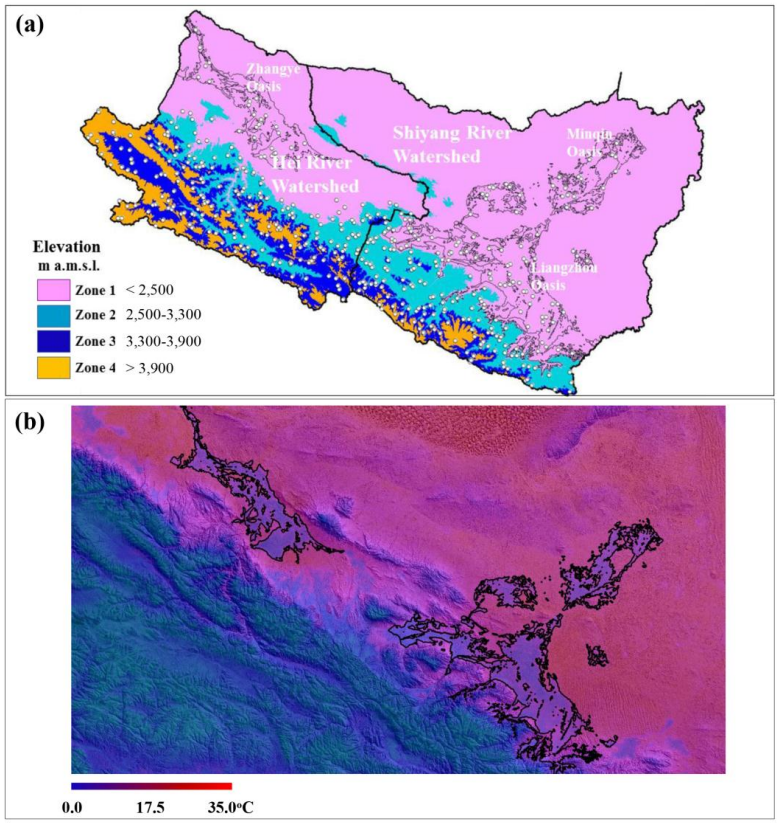

Fig. 2

Formatted: Centered

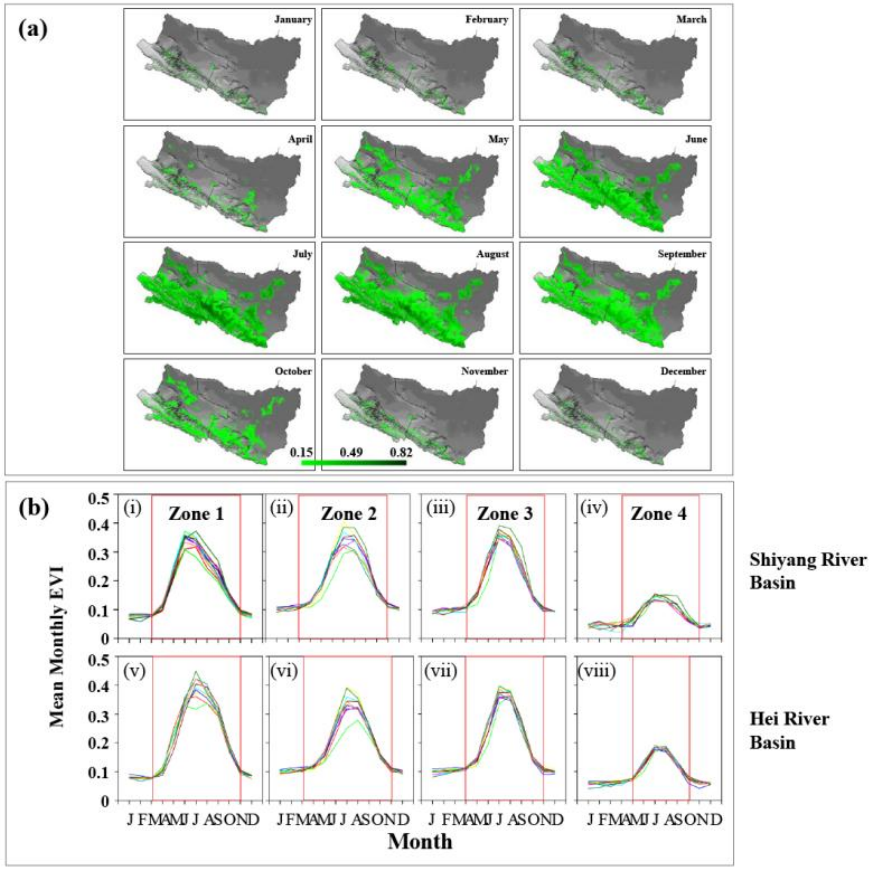

Fig. 3

Formatted: Centered

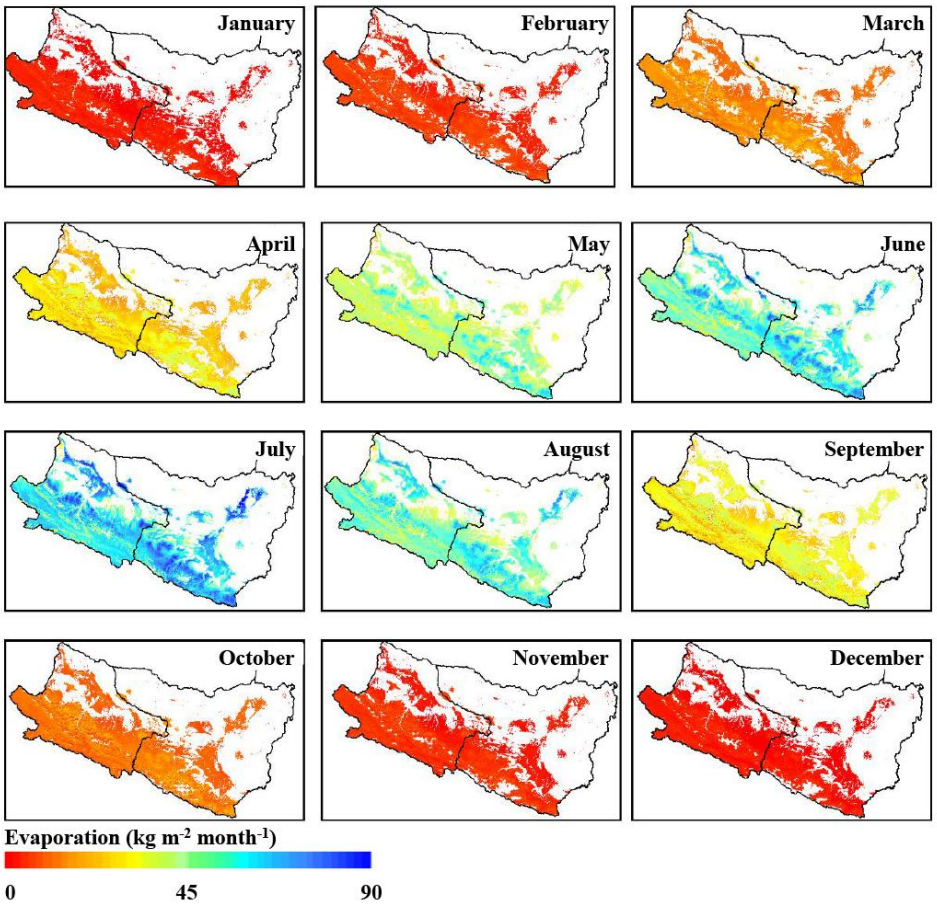

Formatted: Centered

Fig. 4

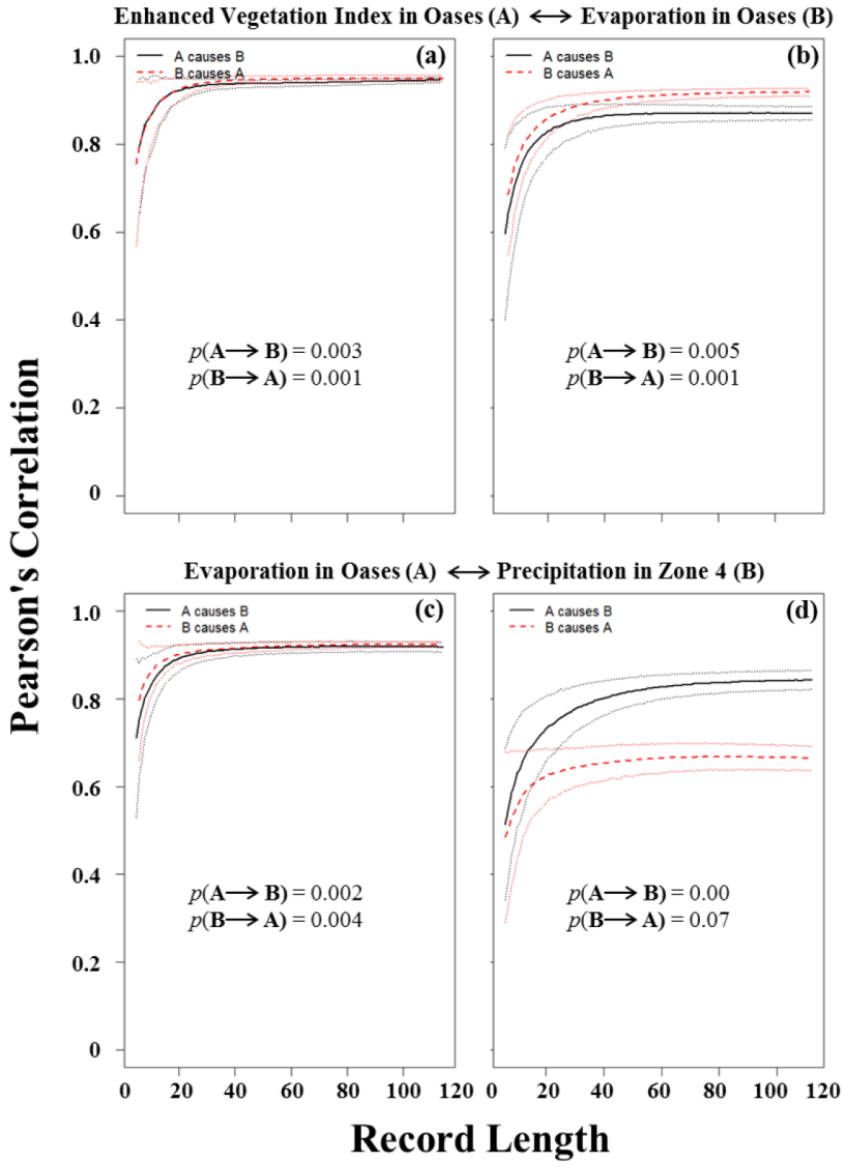
Enhanced Vegetation Index in Oases (A) ⟷ Evaporation in Oases (B)
Evaporation in Oases (A) ⟷ Precipitation in Zone 4 (B)
Pearson's Correlation
Record Length
A causes B
B causes A
(a)
(b)
(c)
(d)
p(A⟶ B) = 0.003
p(B⟶ A) = 0.001
p(A⟶ B) = 0.005
p(B⟶ A) = 0.001
p(A⟶ B) = 0.002
p(B⟶ A) = 0.004
p(A⟶ B) = 0.00
p(B⟶ A) = 0.07
1.0
0.8
0.6
0.4
0.2
0
0 20 40 60 80 100 120

Fig. 5

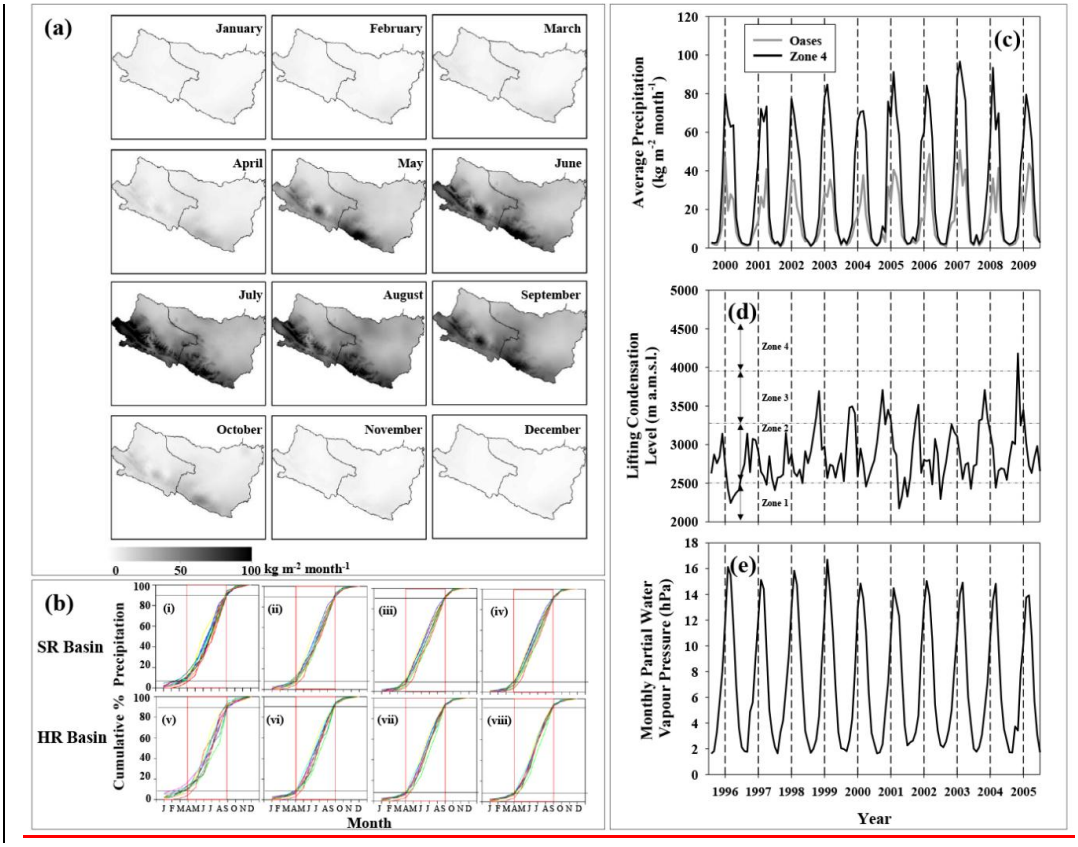
(a)
January
February
March
April
May
June
July
August
September
October
November
December
0
50
100 kg m-2 month-1
(b)
SR Basin
HR Basin
Cumulative % Precipitation
(i)
(ii)
(iii)
(iv)
(v)
(vi)
(vii)
(viii)
J F M A M J J A S O N D
Month
(c)
Oases
Zone 4
Average Precipitation (kg m-2 month-1)
2000 2001 2002 2003 2004 2005 2006 2007 2008 2009
(d)
Zone 4
Zone 3
Zone 2
Zone 1
Lifting Condensation Level (m a.m.s.l.)
(e)
Monthly Partial Water Vapour Pressure (hPa)
1996 1997 1998 1999 2000 2001 2002 2003 2004 2005
Year

Fig. 6

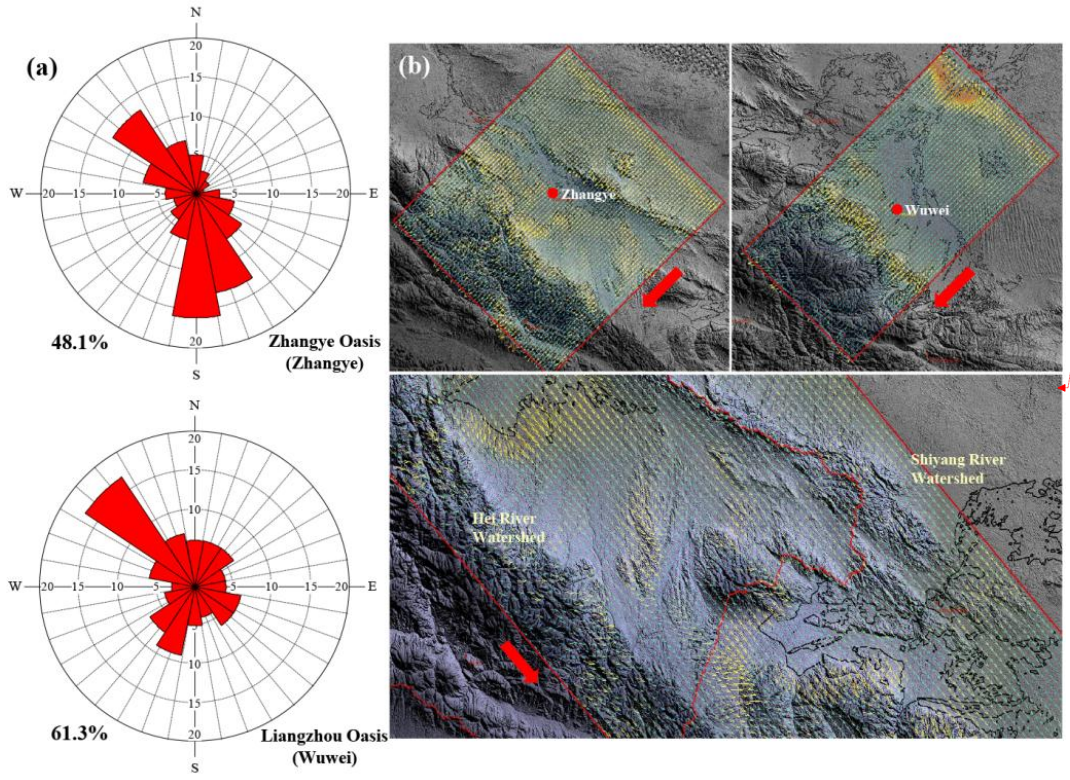

Formatted: Centered

Fig. 7

Formatted: Centered

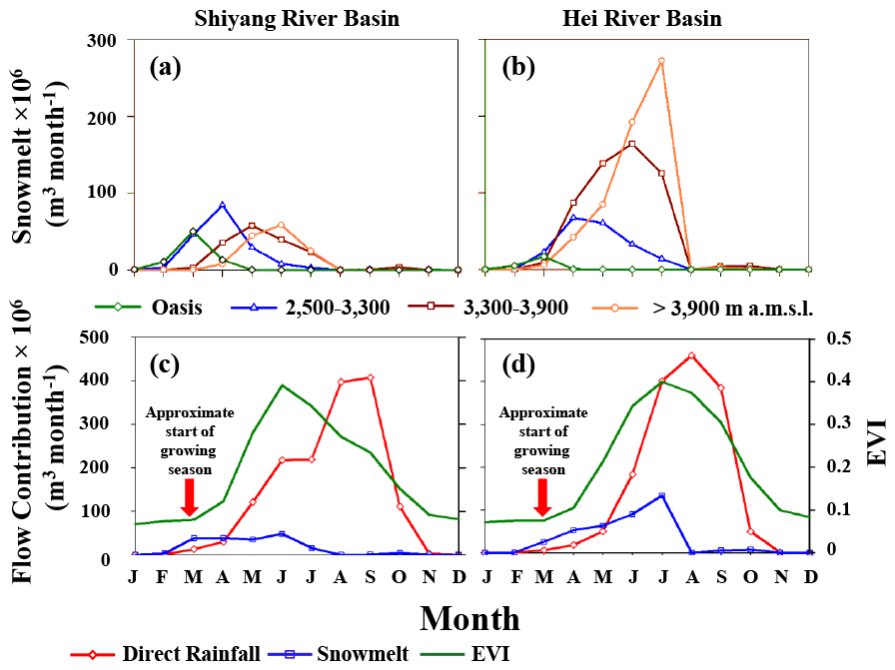

Fig. 8

Formatted: Centered

Table 1. List of weather stations, their coordinates, elevation, and mean total annual precipitation based on measurements from 1976-2005. Stations are located within or near the Hexi Corridor (Fig. 1).

Station ID	Station	Latitude (ºN)	Longitude (ºE)	Elevation (m a.m.s.l.)	Precipitation (kg m^{-2} yr^{-1})
52323	Mazongshan	41.80	97.03	1770	70.6
52418	Dunhuang	40.15	94.68	1140	41.4
52424	Guazhou	40.50	95.92	1177	51.7
52436	Yumen	40.27	97.03	1527	66.5
52446	Dingxin	40.40	99.80	1158	54.7
52447	Jinta	39.82	98.90	1372	62.4
52533	Suzhou	39.77	98.48	1478	85.6
52546	Gaotai	39.37	99.82	1332	110.1
52557	Linze	39.16	100.16	1454	111.7
52652	**Zhangye**[a]	**38.93**	**100.43**	**1483**	**129.8**
52679	**Wuwei**	**37.92**	**102.67**	**1534**	**170.7**
52681	Minqin	38.63	103.08	1367	112.9

[a] Stations in bold are those found in the Zhangye and Liangzhou Oases, refer to Fig. 1.

Table 2. Input variables and their image-data sources relevant to the generation of evaporation, precipitation, and snowmelt surfaces addressed in this study, including their spatiotemporal resolutions (columns 3 and 4) before and after spatial enhancement. Bracketed values are not given in cases where there is no spatial enhancement or temporal aggregation used (modified after Matin and Bourque, 2013a).

Variables	Product generation or source	Spatial	Temporal
		Original (after processing)	Original (after processing)
Normalised difference vegetation index (NDVI)[a] Enhanced vegetation index (EVI)[a,b]	MODIS vegetation indices (Huete et al., 2002; Huete et al., 1997; Wan et al., 2004).	250 m	16 day (1 month)
Land surface temperature (T_s)[a,b]	MODIS land surface temperature (MOD11A2; Wan et al., 2004); monthly averages were produced by weighted averaging of 8-day composites. The original 1000-m resolution was enhanced to 250 m using MODIS EVI (at 250-m resolution) as primary predictor; processing steps are outlined in section 3.2.1 (steps 1-6; in Matin and Bourque, 2013a).	1,000 m (250 m)	8 day (1 month)
Land surface emissivity (ε_s)[a]	MODIS land surface emissivity was derived by averaging MODIS-bands 31 and 32 emissivities (Petitcolin and Vermote, 2002).	1,000 m	8 day (1 month)
Land surface albedo (A_s)[a]	MODIS products combined with BRDF-albedo products (MCD43B3; Davidson and Wang, 2005).	1,000 m	16 (1 month)
Surface dry-bulb air temperature (T_{dry})[a,b] Surface dew-point temperature (T_{dew})[a,b]	MODIS atmospheric profile data (MOD07; Seeman et al., 2006); near surface air temperature are extracted at the pressure level closest to the ground-surface described by the region's digital elevation model (DEM). Daily data were averaged to generate monthly averages. Original T_{dry}-images were digitally enhanced to 250 m by relating their values to enhanced T_s images; 5000-m resolution images of MODIS-T_{dew} were enhanced to 250 m by relating to MODIS-EVI (250 m) and enhanced T_s. Both T_{dry} and T_{dew} were calibrated and validated against independent climate-station data (Matin and Bourque, 2013a).	5,000 m (250 m)	1 day (1 month)
Surface relative humidity[b]	Relative humidity (250-m resolution) was calculated as the ratio of actual vapour pressure to saturated vapour pressure calculated from monthly T_{dry} and T_{dew} (Bourque and Hassan, 2009), both at 250-m resolution.	250 m	1 month
Total precipitable water[b]	MODIS near infrared daily total precipitable water product (MOD05; Gao and Kaufman, 2003; Kaufman and Gao, 1992); monthly values were generated by averaging daily values.	1,000 m	1 day (1 month)
Elevation[a,b]	Shuttle Radar Topographic Mission (SRTM) DEM; gap-filled version (v. 4) obtained from the Consortium of Spatial Data and Information (CGIAR-CSI, 2008; Reuter et al., 2007).	90 m	n/a[c]

Net radiation and soil heat flux (i.e., R_n-G)[a]	Calculated from estimated incoming solar radiation obtained with the Solar Analyst tool in ArcGIS and SRTM DEM-elevation data, and remote sensing-based A_s, T_{dry}, and T_s images in estimating outgoing and incoming reflected shortwave and longwave radiation surfaces for R_n and a NDVI-based correction of incident solar radiation for the ground heat flux (G; see Matin and Bourque, 2013b).	250 m	n/a

[a] Variables used in the calculation of evaporation; [b] ~~variables~~ Variables used in the digital enhancement of TRMM-precipitation data (Matin and Bourque, 2013a); [c] n/a=not applicable.

Table 3. Regression fits (y=mx+b; m=slope and b=y-intercept) and their associated coefficients of determination (r^2) for comparisons between basin-level monthly evaporation over a 10-year period (2000-2009) as a function of same-month enhanced vegetation index -for different vegetated-cover types (subset of landcover types in Table A1 and Fig. 1). Vegetated-cover types are ordered according to their position in the basins (Fig. 1), starting with vegetation types in Zone 1 (< 2,500 m a.m.s.l.).

Landcover Type	**Shiyang River Basin**			**Hei River Basin**		
	m	**b**	**r^2**	**m**	**b**	**r^2**
Crops	175.87	-6.92	0.85	157.47	-3.5	0.84
Dense grass in oases	175.84	-8.32	0.83	170.06	-7.78	0.73
Sparse grass and/or shrubs	218.23	-2.97	0.54	214.39	-1.1	0.49
Alpine meadow	83.80	16.18	0.32	90.57	12.82	0.41
Coniferous forest	74.77	22.58	0.27	97.46	15.57	0.39
Deciduous shrubs	46.26	23.81	0.12	79.21	16.56	0.42

Table 4. Coefficients of determination (r^2) for comparisons between zone-specific precipitation (zones associated with column 1) with same-month, same-zone, or oasis enhanced vegetation index (EVI) and evaporation (E; zones associated with row 1) for the Shiyang and Hei River basins, respectively. Cells associated with comparisons that were not addressed in the analysis, are marked with a "-". Values of r^2 that are in bold are derived for comparisons between zone-specific precipitation with same-month, same-zone EVI and E; values not in bold, are for comparisons between zone-specific precipitation with same-month oasis EVI and E.

Elevation Zone[a]		**1**		**2**		**3**		**4**	
	River Basin	**EVI**	**E**	**EVI**	**E**	**EVI**	**E**	**EVI**	**E**
1	Shiyang River	**0.44**	**0.41**	-	-	-	-	-	-
	Hei River	**0.51**	**0.39**	-	-	-	-	-	-
2	Shiyang River	0.54	0.52	**0.61**	**0.34**	-	-	-	-
	Hei River	0.68	0.56	**0.62**	**0.34**	-	-	-	-
3	Shiyang River	0.61	0.55	-	-	**0.52**	**0.20**	-	-
	Hei River	0.78	0.68	-	-	**0.69**	**0.43**	-	-
4	Shiyang River	0.65	0.57	-	-	-	-	**0.44**	**0.18**
	Hei River	0.85	0.77	-	-	-	-	**0.75**	**0.47**

[a] Zones are classified according to elevation bands: < 2,500 m (Zone 1); 2,500-3,300 m (Zone 2); 3,300-3,900 m (Zone 3); and > 3,900 m a.m.s.l. (Zone 4);

Table 5. Evaporation as a ~~%~~ percentage of the annual sum of ~~precipitation~~ direct rainfall (P) and snowmelt volumes (S) for individual elevation zones and mountain area within the Shiyang and Hei River basins~~,~~ and for the entire river basin, respectively. Percentages are based on ten-year sums.

Elevation Zone[a]	**Evaporation (% [P+S])**	
	Shiyang River Basin	**Hei River Basin**
1	136	210
2	88	100
3	58	81
4	35	62
Entire Mountain Area	72	81
Entire River Basin	90	89

[a] Zones are classified according to elevation bands, i.e., < 2,500 m (Zone 1); 2,500-3,300 m (Zone 2); 3,300-3,900 m (Zone 3); and > 3,900 m a.m.s.l. (Zone 4).